REFERENCES

1) Watanabe, T., Hasei, T., Takahashi, T., Asanoma, M., Murahashi, T., Hirayama, T. and Wakabayashi, K. (2005) Detection of a novel mutagen, 3,6-dinitrobenzo[*e*]pyrene, as a major contaminant in surface soil in Osaka and Aichi prefectures, Japan. *Chem. Res. Toxicol.*, **18**, 283–289.
2) Watanabe, T., Takahashi, K., Konishi, E., Hoshino, Y., Hasei, T., Asanoma, M., Hirayama, T. and Wakabayashi, K. (2008) Mutagenicity of surface soil from residential areas in Kyoto city, Japan, and identification of major mutagens. *Mutat. Res.*, **649**, 201–212.
3) Tokiwa, H. and Onishi, Y. (1986) Mutagenicity and carcinogenicity of nitroarenes and their sources in the environment. *Crit. Rev. Toxicol.*, **17**, 23–60.
4) Kawanishi, M., Watanabe, T., Hagio, S., Ogo, S., Shimohara, C., Jouchi, R., Takayama, S., Hasei, T., Hirayama, T., Oda, Y. and Yagi, T. (2009) Genotoxicity of 3,6-dinitrobenzo[*e*]pyrene, a novel mutagen in ambient air and surface soil, in mammalian cells in vitro and in vivo. *Mutagenesis*, **24**, 279–284.
5) Hasei, T., Watanabe, T. and Hirayama, T. (2006) Determination of 3,6-dinitrobenzo[*e*]pyrene in surface soil and airborne particles by high-performance liquid chromatography with fluorescence detection. *J. Chromatogr. A*, **1135**, 65–70.
6) Hasei, T., Watanabe, T., Endo, O., Sugita, K., Asanoma, M., Goto, S. and Hirayama, T. (2009) Determination of 3,6-dinitrobenzo[*e*]pyrene in surface soil and airborne particles, and its possible sources, diesel particles and incinerator dusts. *J. Health Sci.*, **55**, 567–577.
7) Lin, D., Tu, Y. and Zhu, L. (2005) Concentrations and health risk of polycyclic aromatic hydrocarbons in tea. *Food Chem. Toxicol.*, **43**, 41–48.
8) Lin, D., Zhu, L., He, W. and Tu, Y. (2006) Tea plant uptake and translocation of polycyclic aromatic hydrocarbons from water and around air. *J. Agric. Food Chem.*, **54**, 3658–3662.
9) Fiedler, H., Cheung, C. K. and Wong, M. H. (2002) PCDD/PCDF, chlorinated pesticides and PAH in Chinese teas. *Chemosphere*, **46**, 1429–1433.
10) Schlemitz, S. and Pfannhauser, W. (1997) Supercritical fluid extraction of mononitrated polycyclic aromatic hydrocarbons from tea. Correlation with the PAH concentration. *Z. Lebensm. Unters. Forsch.*, **205**, 305–310.
11) Uegaki, R., Eun, H., Kuwahara, M., Ishii, Y., Kobara, Y., Ueji, M., Nakamura, K. and Narita, I. (2001) The fate of dioxins during green tea manufacture. *Shokuhin Eiseigaku Zasshi*, **42**, 154–158.
12) Toriba, A., Kuramae, Y., Chetiyanukornkul, T., Kizu, R., Makino, T., Nakazawa, H. and Hayakawa, K. (2003) Quantification of polycyclic aromatic hydrocarbons (PAHs) in human hair by HPLC with fluorescence detection: A biological monitoring method to evaluate the exposure to PAHs. *Biomed. Chromatogr.*, **17**, 126–132.
13) Kobayashi, M., Hanaoka, T. and Tsugane, S. (2007) Validity of a self-administered food frequency questionnaire in the assessment of heterocyclic amine intake using 2-amino-1-methyl-6-phenylimidazo[4,5-*b*]pyridine (PhIP) levels in hair. *Mutat. Res.*, **630**, 14–19.
14) Hegstad, S., Lundanes, E., Reistad, R., Haug, L. S., Becher, G. and Alexander, J. (2000) Determination of the food carcinogen 2-amino-1-methyl-6-phenylimidazo[4,5-*b*]pyridine (PhIP) in human hair by solid-phase extraction and gas chromatography-mass spectrometry. *Chromatographia*, **52**, 499–504.
15) Ozeki, H., Ito, S., Wakamatsu, K. and Hirobe, T. (1995) Chemical characterization of hair melanins in various coat-color mutants of mice. *J. Invest. Dermatol.*, **105**, 361–366.

Formation of cholesterol ozonolysis products in vitro and in vivo through a myeloperoxidase-dependent pathway

Susumu Tomono,*,§ Noriyuki Miyoshi,[1],*,§ Hidemi Shiokawa,*,§ Tomoe Iwabuchi,*,§ Yasuaki Aratani, Tatsuya Higashi,†,§ Haruo Nukaya,*,§ and Hiroshi Ohshima*,§**

Laboratory of Biochemistry,* Graduate School of Nutritional and Environmental Sciences, Laboratory of Analytical and Bio-Analytical Chemistry,† Graduate School of Pharmaceutical Sciences, and the Global Center of Excellence (COE) Program,§ University of Shizuoka, Shizuoka, Japan; and Graduate School of Nanobioscience,** Yokohama City University, Kanagawa, Japan

Abstract 3β-Hydroxy-5-oxo-5,6-secocholestan-6-al (secosterol-A) and its aldolization product 3β-hydroxy-5β-hydroxy-B-norcholestane-6β-carboxaldehyde (secosterol-B) were recently detected in human atherosclerotic tissues and brain specimens, and they may play pivotal roles in the pathogenesis of atherosclerosis and neurodegenerative diseases. However, as their origin remains unidentified, we examined the formation mechanism, the stability, and the fate of secosterols in vitro and in vivo. About 40% of secosterol-A remained unchanged after 3 h incubation in the FBS-free medium, whereas 20% and 40% were converted to its aldehyde-oxidation product, 3β-hydroxy-5-oxo-secocholestan-6-oic acid, and secosterol-B, respectively. In the presence of FBS, almost all secosterol-A was converted immediately to these compounds. Secosterol-B in the medium, with and without FBS, was relatively stable, but ~30% was converted to its aldehyde-oxidation product, 3β-hydroxy-5β-hydroxy-B-norcholestane-6-oic acid (secoB-COOH). When neutrophil-like differentiated human leukemia HL-60 (nHL-60) cells activated with PMA were cultured in the FBS-free medium containing cholesterol, significantly increased levels of secosterol-A and its aldehyde-oxidation product, but not secosterol-B, were formed. This secosterol-A formation was decreased in the culture of PMA-activated nHL-60 cells containing several reactive oxygen species (ROS) inhibitors and scavengers or in the culture of PMA-activated neutrophils isolated from myeloperoxidase (MPO)-deficient mice. Our results demonstrate that secoterol-A is formed by an ozone-like oxidant generated with PMA-activated neutrophils through the MPO-dependent mechanism.—Tomono, S., N. Miyoshi, H. Shiokawa, T. Iwabuchi, Y. Aratani, T. Higashi, H. Nukaya, and H. Ohshima. **Formation of cholesterol ozonolysis products in vitro and in vivo through a myeloperoxidase-dependent pathway.** ***J. Lipid Res.*** **2011.** 52: **87–97.**

Supplementary key words secosterol • neutrophils • myeloperoxidase • inflammation

A reactive species with a chemical signature similar to that of ozone has been proposed to be generated by the antibody-catalyzed oxidation of water with singlet oxygen during the oxidative burst of activated human neutrophils and in inflamed tissues (1, 2). The formation of an ozone-like oxidant from singlet oxygen by neutrophils can be catalyzed not only by antibodies but also by amino acids such as tryptophan, methionine, and cysteine (3). To prove the formation of an ozone-like oxidant by neutrophils, previous studies used chemical reactions, such as the conversion of indigo carmine to isatin sulfonic acid or the oxidation of vinylbenzoic acid to 4-carboxybenzaldehyde. However, these reactions are not sufficiently specific to ozone to conclude an ozone production by neutrophils (4, 5).

Further evidence for ozone formation in vivo was based on the detection and formation of the cholesterol ozonolysis products 3β-hydroxy-5-oxo-5,6-secocholestan-6-al (secosterol-A, also called atheronal-A) and its aldolization product 3β-hydroxy-5β-hydroxy-B-norcholestane-6β-carboxaldehyde (secosterol-B, also called atheronal-B) in human tissues. These secosterols were previously reported to be formed only by ozone among the various reactive oxygen species (ROS) such as singlet oxygen, superoxide anion, hydroxyl

This work was supported by the Global Centers of Excellence (COE) Program of Japan's Ministry of Education, Science, Culture, and Sport; Grants-in-Aid 18509001 (HO), 21300280 (HO), 19700592 (NM), and 21680052 (NM) from Japan's Ministry of Education, Science, Culture, and Sport; Grants-in-Aid 19-19 and 21-1-2 for Cancer Research from Japan's Ministry of Health, Labor, and Welfare; and Grant KHC1023 and a grant from the Japan Health Science Foundation for Health Sciences Focusing on Drug Innovation.

Manuscript received 11 March 2010 and in revised form 9 August 2010.

Published, JLR Papers in Press, October 4, 2010
DOI 10.1194/jlr.M006775

Abbreviations: α, β-unsaturated-secosterol-B, 3β-hydroxy-B-norcholest-5-ene; DH, dansyl hydrazine; HOCl, hypochlorous acid; LPS, lipopolysaccharide; MPO, myeloperoxidase; nHL-60, neutrophil-like differentiated human leukemia HL-60; PA, 2-picolylamine; PEG, polyethylene glycol; ROS, reactive oxygen species; secoA-COOH, 3β-hydroxy-5-oxo-secocholestan-6-oic acid; secoB-COOH, 3β-hydroxy-5β-hydroxy-B-norcholestane-6-oic acid; secosterol-A, 3β-hydroxy-5-oxo-5,6-secocholestan-6-al; secosterol-B, 3β-hydroxy-5β-hydroxy-B-norcholestane-6β-carboxaldehyde; SOD, superoxide dismutase; WT, wild-type.

[1] To whom correspondence should be addressed.
e-mail: miyoshin@u-shizuoka-ken.ac.jp

radicals, and ozone (6–9). Secosterols were recently detected in human atherosclerotic tissues (10) and in human brain specimens from patients with Alzheimer's disease (11). They were also detected in Lewy body dementia (12) by the analysis of their hydrazine derivatives with LC-MS. Higher concentrations of secosterol-A were detected in the diseased arteries of patients with atherosclerosis. This secosterol-A concentration was further increased upon activation with PMA, suggesting that human leukocytes within atherosclerotic tissues are activated to produce an ozone-like oxidant (10). However, it has been recently reported that secosterol-A and -B were generated in an ozone-independent manner via the Hock-cleavage of 5α-hydroperoxy cholesterol, which can arise from the singlet oxygen ene reaction with cholesterol (13, 14). Secosterol-B is formed easily under acidic conditions in organic solvents (13, 14), whereas secosterol-A is either not formed at all or is a minor component in the aqueous buffer (9). We reported recently that almost equal amounts of secosterol-A and -B were formed by the reaction of cholesterol with human myeloperoxidase (MPO) in the presence of its substrates hydrogen peroxide (H_2O_2) and Cl^- (15). On the other hand, five times more secosterol-B was formed than secosterol-A when cholesterol was incubated with hypochlorous acid (HOCl) and hydrogen peroxide. However, in both the reactions, immunoglobulin G (IgG) did not enhance the formation of secosterols, suggesting that singlet oxygen ($^1O_2$) and possibly another oxidant, but not an ozone-like oxidant, mediated the formation of secosterols (15).

Although the exact mechanism for the formation of secosterols in human tissues remains unidentified, secosterols have been reported to react with the amyloid β protein in Alzheimer's disease, resulting in the misfolding and aggregation of this protein (11, 16, 17), which accelerate amyloidogenesis. Secosterols can also accelerate α-synuclein fibrilization (12), which has been associated with Parkinson's disease and Lewy body dementia (18). Secosterols exert cytotoxic effects on various culture cells (10, 19, 20).

We recently reported a highly sensitive method for the quantification of secosterols based on derivatization with fluorescent dansyl hydrazine (DH) and detection by LC-MS/MS system, in which both secosterols were confirmed to be stable during the derivatization process (15). This sensitive method has allowed us to perform quantitative analysis of secosterols in cell culture and in animal tissues. In this study, we examined the molecular mechanism for the formation of secosterols in vivo. We demonstrate here that the formation of secosterol-A and -B are enhanced by the inflamed stimuli not only in the cultures of neutrophil-like differentiated HL-60 cells or mouse neutrophils, but also in plasma samples and the liver of mice after lipopolysaccharide (LPS) administration. In addition, we have studied the fate of secosterols added to the culture medium with and without FBS. Several products, including 3β-hydroxy-5-oxo-secocholestan-6-oic acid (secoA-COOH), 3β,5β-dihydroxy-B-norcholestane-6-oic acid (secoB-COOH), and 3β-hydroxy-B-norcholest-5-ene (α, β-unsaturated-secosterol-B), were newly identified as metabolites of secosterol-A and -B. On the basis of these findings, we have shown evidence suggesting that the formation of secosterols is mediated by an MPO-dependent system in vivo at least partly through an oxidant with the chemical signature of ozone.

MATERIALS AND METHODS

Materials

Allopurinol, apocynin, cholesterol, 3,4-^{13}C-cholesterol, catalase (bovine), cell permeable catalase, covalently linked to polyethylene glycol (PEG-catalase), superoxide dismutase (SOD) (bovine), PEG-SOD, PMA, immunoglobulin G (bovine serum), *p*-toluenesulfonic acid, sodium azide, and LDL were purchased from Sigma, St. Louis, MO. Dansyl hydrazine (DH) and RPMI 1640 medium were purchased from Invitrogen (Carlsbad, CA) and Nissui Pharmaceutical Co., Ltd., Tokyo, Japan, respectively. All other chemicals were obtained from Wako Pure Chemical Industries, Osaka, Japan.

Synthesis of ozonolysis products of cholesterol

Secosterols and their metabolites were synthesized according to the method reported by Wentworth et al. (10). The purity of the product was verified by TLC and ^{1}H-NMR. The stock solutions (10 mM) of secosterols were prepared in ethanol and stored at −20°C until use.

Fate of secosterols in culture media

One hundred pmol secosterol-A and -B were added into 1 ml of RPMI 1640 medium in the absence or presence of 10% FBS. After the incubation for 0-3 h, the media were spiked with stable isotopes labeled synthesized 3,4-^{13}C-secosterol-A or -B (5 nmol each) and mixed vigorously with 2 ml chloroform-methanol (2:1) for 1 min. After centrifugation at 3,000 rpm for 10 min, the organic phase was separated, washed with water twice, and evaporated to dryness in vacuo. The secosterols were analyzed as described below using a calibration curve prepared with several concentrations of standard compounds.

Formation of secosterols by HL-60 cells

Human leukemia HL-60 cells (RIKEN Cell Bank, Tsukuba, Ibaraki, Japan) were maintained in RPMI 1640 supplemented with 10% heat-inactivated FBS, 2 mM glutamine, 50 U/ml penicillin and 50 μg/ml streptomycin in an atmosphere of 95% air and 5% CO_2 at 37°C. HL-60 cells seeded at 5×10^5 cells/ml were differentiated into neutrophils by the treatment with 1.25% dimethylsulfoxide for 5 days (21). Then the medium was substituted for a fresh one containing either 10% FBS or no FBS. When the FBS-free medium was used, 6 μg/ml IgG and/or 30 μg/ml cholesterol were exogenously added into the medium, as FBS (10%) contained the compounds at these concentrations. The cells were then activated with 10 nM PMA for 0-3 h. When inhibitors of MPO (sodium azide, aminobenzohydrazide and salicylhydroxamic acid) were examined, they were added 1 h before the addition of PMA. Other inhibitors and chemicals were added just prior to the PMA activation. The harvested cells and the culture medium spiked with a stable isotope labeled synthesized 3,4-^{13}C-secosterol-A and -B (5 nmol or 10 pmol each in Figs. 2 and 3, respectively) were mixed with 25 ml chloroform-methanol (2:1). Secosterols were extracted and quantified by external or internal standard methods as shown in Figs. 2 and 3, respectively, as described below. The trace amounts of secosterol-A and -B (about 0.7 and 15 nM, respectively) were always detected in the cell-free culture media containing 10% FBS

(Fig. 2). Similarly, commercially available cholesterol also contained detectable amounts of secosterol-A and -B at the levels of ~7 and 200 μmol/mol cholesterol, respectively.

Animal experiments

Animals used in this study were kept according to guidelines for the care and use of laboratory animals at the University of Shizuoka, and all experiments were approved by the local animal ethical committee. *Mpo*$^{-/-}$ mice, backcrossed to a C57BL/6 background 10 times, were genotyped using polymerase chain reaction-amplified DNA from tail clippings (22). Wild-type (WT) male C57BL/6 control mice were obtained from the Japan SLC (Hamamatsu, Japan). Neutrophils were isolated from the bone marrow of the untreated WT and *Mpo*$^{-/-}$ mice (11 weeks of age) using the Percoll (Sigma) density gradient isolation method. Isolated neutrophils, with over 95% purity and viability confirmed by the trypan blue exclusion assay and the HE stain, were suspended in RPMI 1640 in the presence or absence of 10% FBS. After the PMA stimuli for 3 h, the cells and medium were harvested and then mixed with 4 ml chloroform-methanol (2:1) containing stable isotope labeled synthesized 3,4-^{13}C-secosterol-A and -B (10 pmol each). Secosterols extracted were derivatized and analyzed by LC-MS/MS as described below. The levels of secosterols were determined in the plasma samples of mice (6-7 weeks of age, n = 2-4 in each group), which had been treated with or without an intraperitoneal injection of 30 mg/kg body weight of *E. coli* LPS. At 6 or 22 h after LPS administration, the mice were euthanized, and blood samples were obtained with a heparinized syringe from the inferior vena cava. The plasma samples were stored at −80°C until analysis. 3,4-^{13}C-Secosterol-A and -B (10 pmol each) were added to 20 μl of plasma before being mixed with 100 μl chloroform-methanol (2:1). Then the secosterols were analyzed by LC-MS/MS as described below. Under these conditions, the recoveries of secosterol-A and -B (10 pmol each) were 100.1 and 101.3%, respectively.

Analysis of secosterols by LC-MS/MS

The secosterols -A, -B, and α, β-unsaturated-secosterol-B (structures, see Fig. 7) were analyzed after derivatization with DH as described in our previous study (15). Briefly, aliquots of extracted samples from the culture media or animal tissues were dissolved in acetonitrile containing 0.5 mg/ml DH and 0.1 mg/ml *p*-toluensulfonic acid, and derivatized for 4 h at room temperature in darkness. The derivatized mixture was evaporated to dryness in vacuo, and the residue was finally dissolved in 1 ml acetonitrile. SecoA-COOH and SecoB-COOH (structures, see Fig. 7) were analyzed by LC-MS/MS after derivatization with 2-picolylamine (PA) (23). Briefly, aliquots of extracted samples were dissolved in acetonitrile (100 μl). Then, freshly prepared solutions of triphenylphosphine (10 mM) in acetonitrile (10 μl), 2,2′-dipyridyl disulfide (10 mM) in acetonitrile (10 μl) and PA (10 μg) in acetonitrile (10 μl) were successively added, and the mixture was incubated at 60°C for 10 min. After removal of the solvent in vacuo, the products were dissolved in 1 ml acetonitrile. A 10 μl aliquot from each individual sample was used for LC-MS/MS analysis. LC-MS/MS analyses, using nanospace SI-1 (SHISEIDO Co., Ltd., Tokyo, Japan) and API2000™ (Applied Biosystems, Forester City, CA) were performed with an electrospray ionization device running in a positive ionization mode. The derivatives were separated using a TSK-GEL ODS-100V column (150 × 2.0 mm, 3 μm TOSOH, Tokyo, Japan) with a linear gradient of 70% solvent A (0.1% formic acid in water) and 30% solvent B (acetonitrile containing 0.1% formic acid) to 100% solvent B in 20 min, followed by 100% solvent B for 20 min at the flow rate of 0.2 ml/min, and analyzed in MRM mode. The ion transitions monitored for DH derivatives of secosterol-A and -B were *m/z* 666.5/170.2, 236.1; those of 3,4-^{13}C-secosterol-A and -B were *m/z* 668.5/170.2, 236.1; that of α, β-unsaturated-secosterol-B was *m/z* 648.4/170.0, 365.1; and the PA-derivatives of secoA-COOH and secoB-COOH were *m/z* 525.4/109.1, 381.4.

RESULTS

Fate of secosterol-A and -B in the culture medium with and without 10% FBS

We determined the stability and fate of secosterol-A and -B exogenously added to the culture medium in the presence and absence of 10% FBS. When we initially examined the stability of secosterols in culture media, we employed 10 pmol of 3,4-^{13}C-secosterol-A or -B as an internal standard, which resulted in a poor total recovery of compounds (20-40%) (data not shown). However, when 500 times more 3,4-^{13}C-secosterol-A or -B (5 nmol each) were added before lipid extraction with chloroform-methanol, their total recovery was markedly improved and reached between 75% and 100%. This increased recovery could be due to the replacement by excess 3,4-^{13}C-secosterol-A or -B of initially added secosterols, which were probably present as reversibly bound forms with medium components. Using these improved conditions, we found that almost all secosterol-A added to the FBS-containing medium disappeared very rapidly, and 60-80% of secosterol-A was immediately converted to secosterol-B (**Fig. 1A**). We also observed that smaller parts of secosterol-A were converted to the aldehyde-oxidation products of secosterols, secoA-COOH and secoB-COOH (18% and 3%, respectively). In contrast, secosterol-A added to the FBS-free medium disappeared relatively slowly compared with the FBS-containing medium (Fig. 1B). About 40%, 38%, and 17% of added secosterol-A were detected as an unchanged compound, secosterol-B and secoA-COOH, respectively, after 3 h incubation (Fig. 1B). Conversely, it was found that about 60% of the original amount of secosterol-B remained unchanged in 10% FBS-containing medium, but 20% and 0.8% of secosterol-B were converted immediately to secoB-COOH and α, β-unsaturated-secosterol-B, respectively (Fig. 1C). No further increase or decrease of these compounds was observed during a period of 3 h incubation (Fig. 1C). The stability and the fate of secosterol-B added to the FBS-free medium was similar to that observed in the 10% FBS-containing medium (Fig. 1D). No conversions of secosterol-B to secosterol-A were detected during incubation in the media, both with and without FBS (Fig. 1C, D). In addition to these metabolites, we also detected small peaks with *m/z* values corresponding to other secosterol metabolites, including dehydrated derivatives of secoA-COOH and secoB-COOH (data not shown). Our results indicate that secosterol-A is very rapidly converted mainly to secosterol-B and secoA-COOH by some components in FBS, and some parts of secosterol-B are converted to secoB-COOH by some constituents in the culture medium.

Formation of secosterol-A and -B by neutrophil-like differentiated HL-60 cells

On the basis of the above findings, we examined the molecular mechanism for the formation of secosterols by

ASBMB JOURNAL OF LIPID RESEARCH JLR

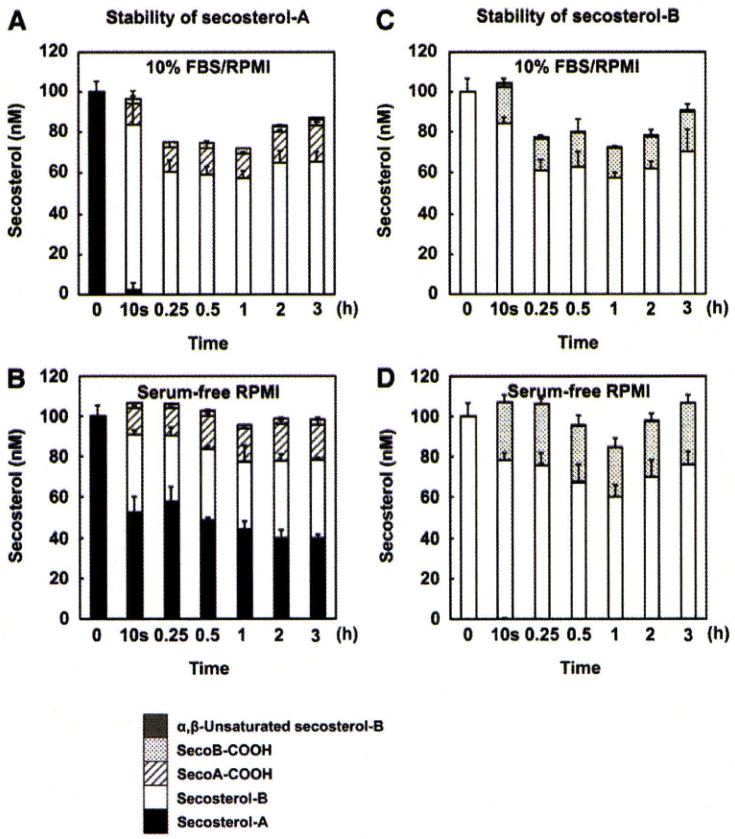

Fig. 1. Comparison of the stability and fate of secosterol-A and secosterol-B incubated in the culture medium with 10% FBS or without FBS. 100 pmol of synthesized secosterol-A (A and B) or secosterol-B (C and D) were incubated in 1 ml of the medium. At the indicated time, lipid fractions from harvested samples were extracted in the presence of excess 3,4-^{13}C-secosterol-A or -B (5 nmol), derivatized with DH or PA, and then analyzed as described in the text. Values are means ± SD (n = 3). DH, dansyl hydrazine; PA, 2-picolylamine; secosterol-A, 3β-hydroxy-5-oxo-5,6-secocholestan-6-al; secosterol-B, 3β-hydroxy-5β-hydroxy-B-norcholestane-6β-carboxaldehyde; secoA-COOH, 3β-hydroxy-5-oxo-secocholestan-6-oic acid; SecoB-COOH, 3β-hydroxy-5β-hydroxy-B-norcholestane-6-oic acid; α, β-unsaturated-secosterol-B, 3β-hydroxy-B-norcholest-5-ene.

cultured neutrophil-like differentiated HL-60 (nHL-60) cells with or without PMA activation. When nHL-60 cells were incubated with 10 nM PMA for 3 h in the FBS-free medium into which cholesterol and IgG were added, significantly elevated levels of secosterol-A but not secosterol-B were formed (**Fig. 2A**, B). Moreover, increased levels of the aldehyde-oxidation products of secosterols, secoA-COOH and secoB-COOH, and α, β-unsaturated-secosterol-B were detected in the cholesterol-containing FBS-free medium (Fig. 2C-E). The formation of secosterol-A but not secosterol-B by the activated nHL-60 cells in the FBS-free medium occurred in a time-dependent manner as well as in the concentration-dependent manner of cholesterol or IgG added to the culture medium (**Fig. 3A, B**). No increased formations of secosterol-A were detected when BSA or heat-inactivated IgG were used in the place of IgG (Fig. 3C). Furthermore, heat-inactivated nHL-60 cells (activated with PMA) lost their ability to produce secosterol-A, even in the presence of IgG and cholesterol in the FBS-free medium (Fig. 3C). Additionally, levels of secosterol-A but not secosterol-B increased significantly (about 2-fold) when the FBS-free medium containing exogenous LDL was incubated with PMA-activated nHL-60 cells (data not shown). On the other hand, when the nHL-60 cells were incubated in the culture medium containing 10% FBS and upon activation with 10 nM PMA for 3 h, an increased level of secosterol-B but not secosterol-A was observed (Fig. 2A, B). When the nHL-60 cells were treated with PMA in the culture medium containing 10% FBS, the amounts of secosterol-B were also increased dose-dependently with increasing concentrations of PMA (up to 10 nM) and in a time-dependent manner (up to 3 h of incubation) (data not shown). Furthermore, the increased formations of secoA-COOH and secoB-COOH are clearly correlated with secosterol-A and secosterol-B formation, respectively (Fig. 2C, D). These results indicate that a major part of secosterol-A produced by the activated nHL-60 cells was immediately metabolized to its oxidation products and secosterol-B by components present in FBS.

Effects of inhibitors, scavengers, and antioxidants on PMA-induced secosterol formation

To elucidate the underlying molecular mechanisms for the formation of secosterols, we examined the effects of various enzyme inhibitors, the scavengers of reactive species, and antioxidant enzymes on secosterol-A formation by PMA-activated nHL-60 cells in the serum-free culture medium to which cholesterol and IgG were exogenously added (**Table 1**). It was found that apocynin (a NADPH oxidase inhibitor), allopurinol (an inhibitor for a xanthine oxidase and a free radical signal generated by activated neutrophils), and MPO inhibitors (sodium azide, aminobenzohydrazide, and salicylhydroxamic acid) significantly inhibited the secosterol-A formation. Similarly, methionine and β-carotene (singlet oxygen scavengers) as well as vinylbenzoic acid (a scavenger for ozone and possibly other reactive species) significantly inhibited

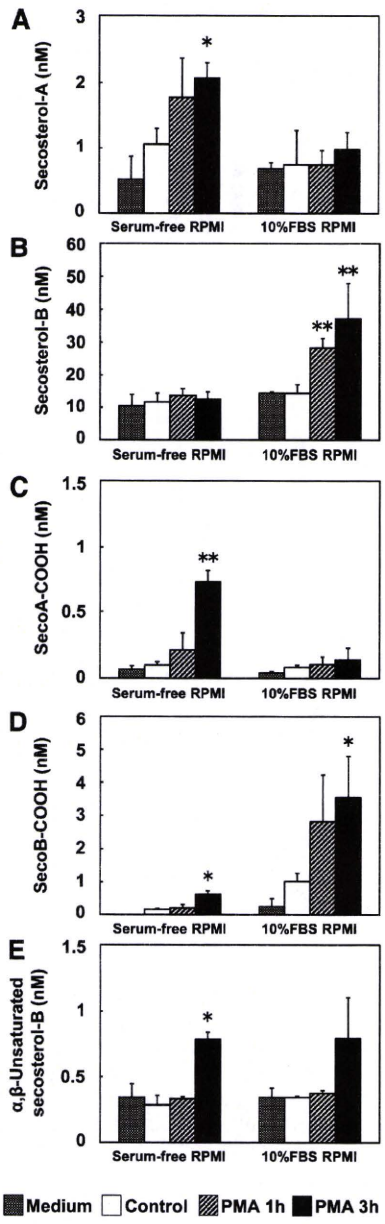

Fig. 2. Formation of secosterols and their oxidation products by nHL-60 cells in the presence or absence of FBS. nHL-60 cells were treated with 0.1% v/v ethanol (control) or 10 nM PMA in ethanol for 1 or 3 h in a serum-free medium containing 30 μg/ml cholesterol and 6 μg/ml IgG or in 10% FBS-medium. Lipid fractions extracted from the harvested cells and the medium were derivatized with DH or PA. Secosterol-A (A), secosterol-B (B), secoA-COOH (C), secoB-COOH (D), and α, β-unsaturated-secosterol-B (E) were analyzed as described in the text. Values are means ± SD (n = 5). Statistically significant: $*P < 0.05$, $**P < 0.01$ versus control. DH, dansyl hydrazine; nHL-60, neutrophil-like differentiated human leukemia HL-60; PA, 2-picolylamine; secoA-COOH, 3β-hydroxy-5-oxo-secocholestan-6-oic acid; secoB-COOH, 3β-hydroxy-5β-hydroxy-B-norcholestane-6-oic acid; secosterol-A, 3β-hydroxy-5-oxo-5,6-secocholestan-6-al; secosterol-B, 3β-hydroxy-5β-hydroxy-B-norcholestane-6β-carboxaldehyde.

secosterol-A formation. Cell permeable catalase, covalently linked to polyethylene glycol (PEG-catalase) alone or PEG-catalase together with PEG-SOD added into the culture medium significantly decreased the amounts of secosterol-A formed by the activated nHL-60 cells, whereas neither PEG-SOD, SOD, nor catalase showed the inhibitory effects on its formation. Similar to the above findings, the formation of secosterol-B by the PMA-activated nHL-60 cells in the 10% FBS-containing medium was effectively inhibited by the same compounds as described above, including inhibitors for NADPH oxidase, xanthine oxidase, and MPO; the scavengers of reactive species such as methionine, β-carotene, and vinylbenzoic acid; PEG-catalase alone, and PEG-catalase plus PEG-SOD (Table 1). These results imply that several reactive species are involved in the formation of secosterols in the culture of PMA-activated nHL-60 cells.

Formation of secosterols by activated neutrophils obtained from wild-type and MPO-deficient mice

As our previous study (15) and the experimental results above suggested the involvement of MPO in the formation of secosterols by activated neutrophils, we employed neutrophils obtained from WT and MPO-deficient mice. Similar to the findings with the PMA-activated nHL-60 cells, cultured WT neutrophils upon activation with PMA significantly produced secosterol-A and -B in the medium containing no FBS (but containing exogenously added cholesterol and IgG) or 10% FBS, respectively (**Fig. 4A**, B). However, no increased formation of secosterol-A or -B was found when PMA-activated neutrophils from MPO-deficient mice were incubated under the same conditions as WT neutrophils (Fig. 4A, B).

Presence of secosterols in plasma and liver of WT and MPO-deficient mice

We determined the levels of secosterols in the samples of plasma and liver collected from WT and MPO-deficient mice. **Fig. 5** shows typical chromatograms obtained for the analyses of secosterols in mice plasma. The background levels of secosterol-A and -B were significantly lower in the plasma samples of MPO-deficient mice than WT mice (**Fig. 6A, B**). Similarly, the levels of secosterol-B detected in homogenates of the liver were also significantly lower in MPO-deficient mice than in WT mice (Fig. 6C). To examine the effect of an acute inflammation stimulus on the formation of secosterols, the mice were injected intraperitoneally with LPS. As shown in Fig. 6A and B, the levels of secosterol-A and -B in the plasma samples collected from WT mice were increased time-dependently after LPS injection, whereas the plasma levels of secosterols in MPO-deficient mice did not increase even after LPS injection.

DISCUSSION

Currently there are two proposed mechanisms for the secosterol formation in vivo: *a)* the oxidation of cholesterol with an ozone-like oxidant to generate secosterol-A and its conversion to secosterol-B by aldolization (2, 10); and *b)* the formation of 5α-hydroperoxy cholesterol by the reaction of cholesterol with singlet oxygen and its Hock-

JOURNAL OF LIPID RESEARCH ASBMB

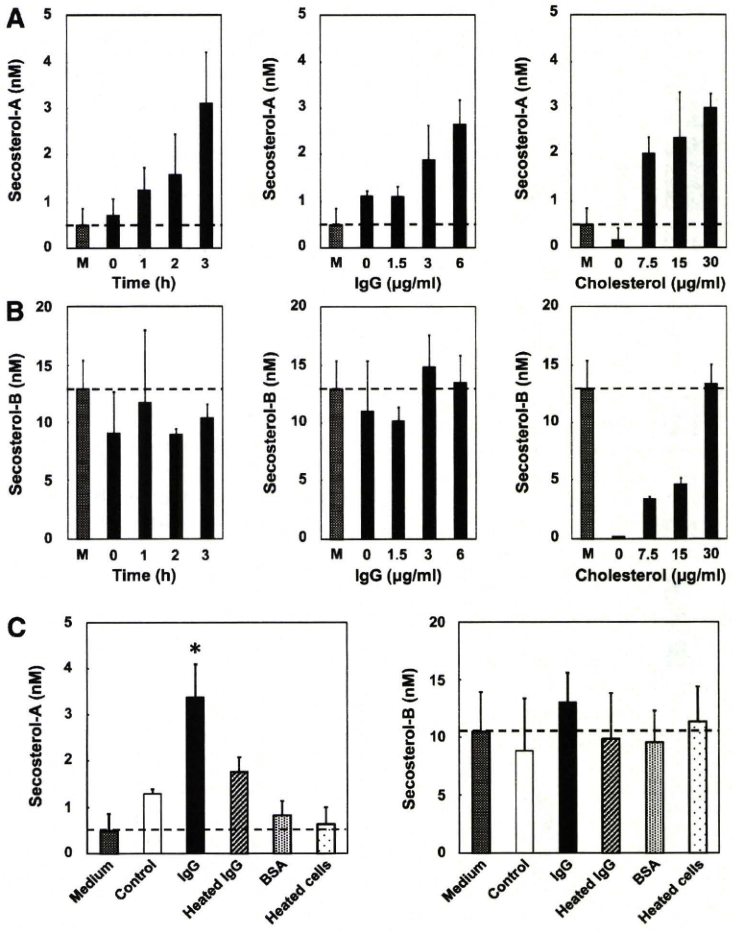

Fig. 3. Effects of incubation time and concentrations of IgG and cholesterol on the formation of secosterol-A and secosterol-B by PMA-activated nHL-60 cells. A, B: nHL-60 cells were incubated with 10 nM PMA in the presence of 30 μg/ml cholesterol or 6 μg/ml IgG for 3 h or indicated modified condition. Secosterols were extracted from the harvested cells and medium, and then analyzed as described in the text. The gray bar (M; medium) and dotted lines represent the levels of preformed secosterols detected in serum-free medium containing 30 μg/ml cholesterol or 6 μg/ml IgG. C: Comparison of formations of secosterol-A and secosterol-B by activated nHL-60 cells in the absence or presence of IgG (6 μg/ml), heat-inactivated IgG (6 μg/ml heated at 100°C for 5 min), and BSA (6 μg/ml). Heat-inactivated nHL-60 cells (100°C, 5 min) were also incubated in the FBS-free medium containing cholesterol and IgG in the presence of PMA. Values are means ± SD (n = 3). Statistically significant: $*P < 0.05$ when compared with control (C). Dotted lines represent the levels of preformed secosterols in the FBS-free medium containing cholesterol. nHL-60, neutrophil-like differentiated human leukemia HL-60; secosterol-A, 3β-hydroxy-5-oxo-5,6-secocholestan-6-al; secosterol-B, 3β-hydroxy-5β-hydroxy-B-norcholestane-6β-carboxaldehyde.

cleavage to generate both secosterol-A and secosterol-B (13, 14). However, recently Wentworth et al. (9) reported that only ozone can react with cholesterol to form secosterol-A and that other oxidants, such as singlet oxygen, form secosterol-B but not -A as a major component. In the present study, we investigated the underlying molecular mechanism for the formation of secosterols by PMA-activated human neutrophil-like HL-60 cells in culture and in mice in vivo.

When we initially determined the stability and the fate of secosterols added to the culture medium, we could identify only 20-40% of the added compounds. However, the total recovery was markedly improved to 75-100% when 500 times more 3,4-^{13}C-secosterol-A or -B were added to the medium before lipid extraction with chloroform-methanol. This might be due to excess 3,4-^{13}C-secosterol-A or -B replacing the previously added secosterols, which could be present as reversibly bound forms with medium components. Using this method, it was found that secosterol-A added to the FBS-free medium decreased more slowly than in the FBS-containing medium, and 40% remained unchanged during 3 h incubation. Conversely, secosterol-A added to the FBS-containing medium immediately disappeared. In contrast, although ~30% of secosterol-B added to the FBS-free medium was converted to secoB-COOH, 60-70% of secosterol-B remained unchanged

TABLE 1. Effects of inhibitors for oxidant-generating enzymes, antioxidants, and scavengers of ROS on the formation of secosterols by PMA-activated nHL-60 cells

Treatment	Concentration	Secosterol-A (nM) Formed in FBS-free Medium		% Inhibition[a]	Secosterol-B (nM) Formed in 10% FBS Medium		% Inhibition[a]
Medium alone		0.5 ± 0.4			14.5 ± 0.3		
nHL-60 without PMA treatment		0.8 ± 0.4			20.3 ± 2.2		
nHL-60 with PMA		3.2 ± 1.1[b]			35.8 ± 4.4[b]		
+ apocynin	100 μM	1.0 ± 0.4[c]		91.7	13.9 ± 2.2[d]	>	100
+ allopurinol	100 μM	0.9 ± 0.1[c]		95.8	15.2 ± 3.5[c]	>	100
+ SOD	100 U/ml	3.1 ± 0.3		4.2	39.2 ± 2.2	<	0
+ catalase	1000 U/ml	2.2 ± 0.3[c]		41.7	26.9 ± 14.7		57.4
+ SOD + catalase	100 U / 1000 U/ml	2.8 ± 0.1		16.7	42.5 ± 7.1	<	0
+ PEG-SOD	100 U/ml	2.8 ± 0.5		16.7	42.9 ± 7.0	<	0
+ PEG-catalase	200 U/ml	1.4 ± 0.2[c]		75.0	17.2 ± 2.0[c]	>	100
+ PEG-SOD + PEG-catalase	100 U / 200 U/ml	1.8 ± 0.7[c]		58.3	21.9 ± 0.8[c]		89.7
+ sodium azide	200 μM	0.5 ± 0.4[c]	>	100	15.6 ± 2.9[c]	>	100
+ aminobenzohydrazide	100 μM	0.2 ± 0.1[d]	>	100	18.1 ± 2.9[c]	>	100
+ salicylhydroxamic acid	100 μM	1.8 ± 0.5[c]		58.3	21.6 ± 2.1[c]		91.6
+ methionine	100 μM	0.7 ± 0.3[c]	>	100	7.1 ± 0.1[d]	>	100
+ β-carotene	50 μM	0.5 ± 0.3[c]	>	100	4.6 ± 1.1[d]	>	100
+ vinylbenzoic acid	100 μM	0.6 ± 0.4[c]	>	100	24.9 ± 2.5[c]		70.3

nHL-60 cells were activated with 10 nM PMA for 3 h in the indicated medium in the presence or absence of test compounds. Formation of secosterol-A or secosterol-B was determined in the FBS-free medium containing 30 μg /ml cholesterol and 6 μg/ml IgG, or in the 10% FBS medium, respectively. Values are means ± SD (n = 3). nHL-60, neutrophil-like differentiated human leukemia HL-60; PA, 2-picolylamine; PEG, polyethylene glycol; ROS, reactive oxygen species; SOD, superoxide dismutase.

[a]Percentage of inhibition representing relative inhibitory effect was calculated for the following equation:

$$\%\text{inhibition} = 100 \times \left(1 - \frac{A - C}{B - C}\right)$$

where A is the amount of secosterol formed by the PMA-activated cells in the presence of a test compound; B is the amount of secosterol formed by the PMA-activated cells in the absence of a test compound; and C is the amount of secosterol presented in the cell culture without PMA treatment.

[b]$P < 0.05$ comparing with and without PMA activation.

[c]$P < 0.05$ comparing the presence and absence of a test compound.

[d]$P < 0.01$ comparing the presence and absence of a test compound.

regardless of the presence or absence of FBS. Moreover, we detected small peaks with *m/z* values corresponding to dehydrated products of secoA-COOH and secoB-COOH (5-oxo-secocholestan-6-oic acid and 5β-hydroxy-B-nor-cholestane-6-oic acid, respectively). About 20% of secosterol-A added to the 10% FBS-containing medium remained unidentified. Secosterol-A could be converted to the above minor or unidentified metabolites, or it could be bound to proteins present in the FBS. Further studies are needed to identify the fate of secosterol-A in vivo.

We next examined whether secosterol-A and -B are formed by nHL-60 cells in culture (Fig. 2). In the case of the experiments with the FBS-free medium, we added both cholesterol and IgG in the same concentrations as those present in 10% FBS. It was found that significantly increased amounts of secosterol-A and its oxidation product secoA-COOH, but not secosterol-B, were formed by the incubation of activated nHL-60 cells. Similarly, the formation of secosterol-A was also observed with activated neutrophils isolated from WT mice (Fig. 4). Under these conditions, the formation of secosterol-A was dependent on the concentrations of cholesterol and IgG added exogenously (Fig. 3). Several enzyme inhibitors and scavengers for different reactive species also inhibited the nHL-60 cell-mediated formation of secosterol-A in the FBS-free medium, implying that the activated cells generate superoxide, hydrogen peroxide, hypochlorous acid, and singlet oxygen, all of which are required to form secosterol-A (Table 1). On the basis of these findings, we can speculate that secosterol-A was formed in the FBS-free medium by the reaction of exogenously added cholesterol with an ozone-like oxidant(s) generated from other reactive species (superoxide, hydrogen peroxide, hypochlorous acid, and singlet oxygen) in the presence of IgG. In addition, the greater amount of secosterol-B formation observed in PMA-activated nHL-60 cells or WT mice neutrophil cultures containing 10% FBS could be mainly derived from a Hock-cleavage of 5α-hydroperoxy cholesterol, as it cannot be explained merely by the aldolization of generated secosterol-A.

In addition to our findings showing that secosterol-A or -B added to the culture medium were immediately oxidized to form secoA-COOH or secoB-COOH (Fig. 1), we found for the first time that secoA-COOH and secoB-COOH were formed in the PMA-activated nHL-60 cells culture (Fig. 2). SecoA-COOH has been reported to induce the fibrilization of apolipoprotein C-II (24) and α-synuclein (12). As no data have been available concerning the presence of these oxidized secosterols in vivo, further studies are needed to establish the levels of metabolites of secosterols in in vivo samples.

We previously reported that almost equal amounts of secosterol-A and -B were formed by the reaction of choles-

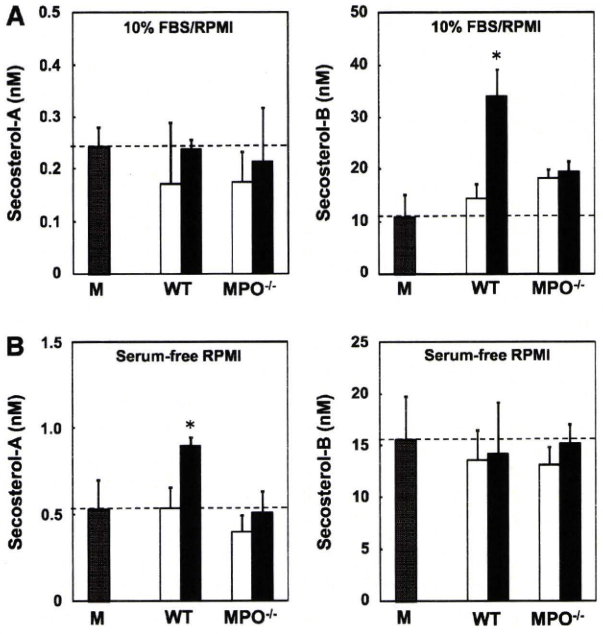

Fig. 4. Formation of secosterols by neutrophils isolated from WT or MPO-deficient mice. Isolated neutrophils were incubated with (closed bars) or without (open bars) 10 nM PMA in the medium without FBS but containing 30 μg /ml cholesterol and 6 μg/ml IgG (A) or containing 10% FBS (B). Values are means ± SD (n = 3). Statistically significant: $^*P < 0.05$ compared the amounts formed by the cells without PMA activation. Dotted lines represent the levels of preformed secosterols in the medium used in each assay. M, medium; MPO, myeloperoxidase; WT, wild-type.

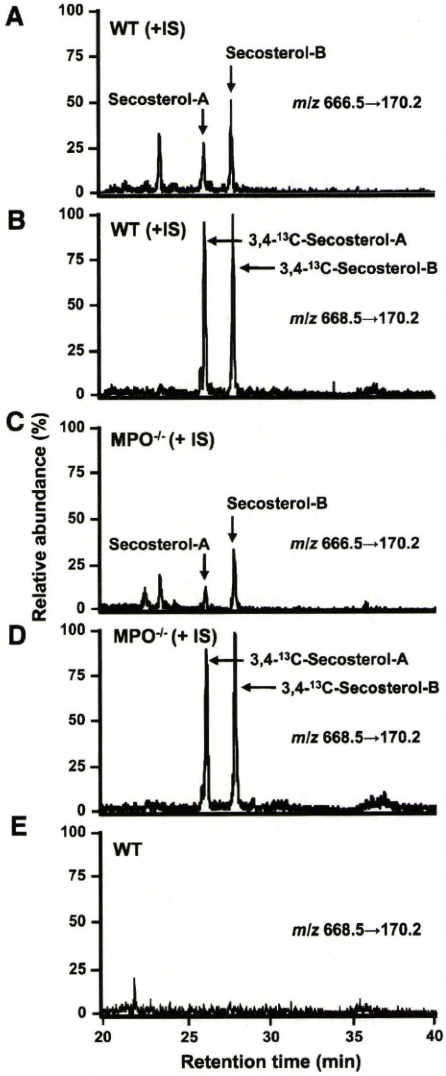

Fig. 5. LC-MS/MS analyses of secosterol-A and secosterol-B in mice plasma. Typical chromatograms obtained by monitoring the ion transition of *m/z* 666.5/170.2 for the DH derivatives of secosterol-A and secosterol-B extracted from a plasma sample of WT mouse (A) and MPO-deficient mouse (C) and 668.5/170.2 for those of internal standards (IS) (3,4-^{13}C-secosterol-A and -B) (B, D). No interfering peaks were detected when the derivatized extract of WT mouse plasma without addition of IS was analyzed for 668.5/170.2 (E). DH, dansyl hydrazine; MPO, myeloperoxidase; secosterol-A, 3β-hydroxy-5-oxo-5,6-secocholestan-6-al; secosterol-B, 3β-hydroxy-5β-hydroxy-B-norcholestane-6β-carboxaldehyde; WT, wild-type.

terol with human MPO in the presence of its substrates hydrogen peroxide and Cl^- (15). The results in this study also indicate that inhibitors of MPO significantly attenuated the formation of secosterols by the PMA-activated nHL-60 cells. These data strongly suggest that MPO is involved in the formation of secosterols. To elucidate the role of MPO, we examined the formation of secosterols by neutrophils isolated from WT and MPO-deficient mice (Fig. 4). It was found that similar to the results obtained with the PMA-activated nHL-60 cells, increased amounts of secosterol-A and -B were formed when PMA-activated neutrophils isolated from WT mice were cultured in the medium without and with 10% FBS, respectively. Interestingly, these increased formations of secosterols were not observed when neutrophils isolated from MPO-deficient mice were cultured under the same conditions. Furthermore, low levels of secosterol-A and -B were detected in the plasma samples and liver obtained from WT mice, whereas their levels were much lower in those obtained from MPO-deficient mice (Fig. 6). Also interestingly, upon the induction of acute inflammation by LPS injection, the plasma levels of both secosterol-A and -B were increased significantly in the WT mice, whereas no increase was found in the MPO-deficient mice. These results clearly indicate that MPO is required for the formation of secosterols in vivo.

We have also shown that the formation of secosterol-A but not -B due to the reaction of cholesterol with PMA-activated nHL-60 cells in the FBS-free medium is enhanced by IgG, but it is decreased by the various enzyme inhibitors and scavengers for different reactive species and by neutrophils from MPO-deficient mice. These results support the notion proposed by Babior et al. (1) and Nieve and Wentworth (2) that a reactive species with a chemical signature similar to that of ozone is generated by activated human neutrophils. On the basis of our results and those of Babior et al. (1) and Nieve and Wentworth (2), we can speculate the following reaction mechanism for the

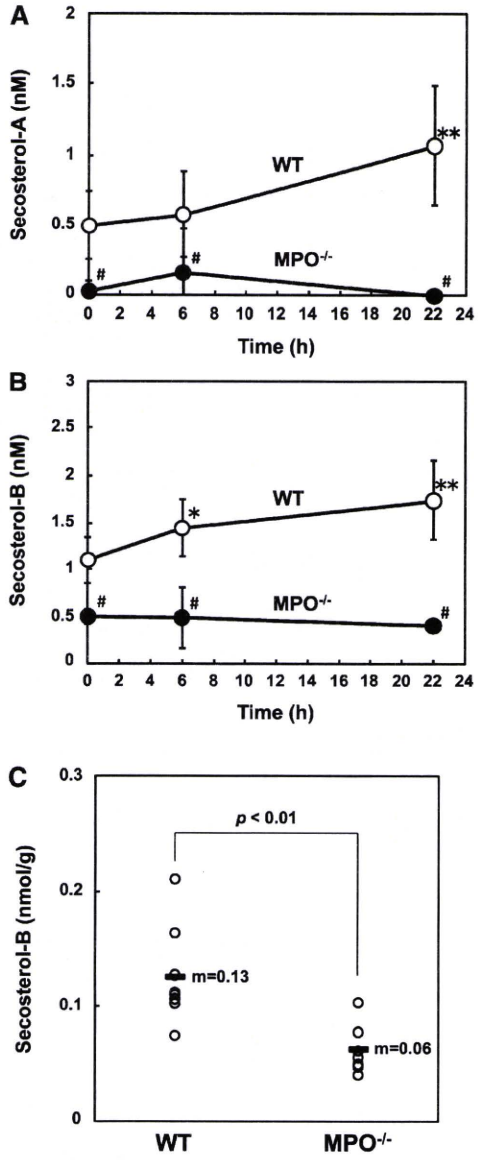

Fig. 6. Levels of secosterols detected in plasma samples and in the liver of WT or MPO-deficient mice. A, B: The levels of secosterol-A and secosterol-B in plasma samples of mice collected at 0, 6 and 22 h after the intraperitoneal injection of LPS (30 mg/kg BW). Values are means ± SD (n = 2-4 in each time point). Statistically significant: $^{*}P < 0.05$, $^{**}P < 0.01$ compared with the levels detected in untreated mice; $^{\#}P < 0.01$ compared with the levels between WT and MPO-deficient mice at each time point. C: The levels of secosterol-B in the liver samples collected from untreated WT (n = 8) and MPO-deficient (n = 7) mice. Median (m) values are presented. LPS, lipopolysaccharide; MPO, myeloperoxidase; secosterol-A, 3β-hydroxy-5-oxo-5,6-secocholestan-6-al; secosterol-B, 3β-hydroxy-5β-hydroxy-B-norcholestane-6β-carboxaldehyde; WT, wild-type; BW, body weight.

formation of secosterol-A by PMA-activated nHL-60 cells in the FBS-free medium: *i*) the activated cells produce superoxide anion by NADPH oxidase and/or xanthine oxidase; *ii*) superoxide is converted to hydrogen peroxide by SOD; *iii*) hydrogen peroxide is used by MPO to generate hypochlorous acid; *iv*) hypochlorous acid in the presence of hydrogen peroxide generates singlet oxygen; *v*) IgG catalyzes the formation of an ozone-like oxidant in the presence of singlet oxygen and hydrogen peroxide; and *vi*) an ozone-like oxidant reacts with cholesterol to form secosterol-A (**Fig. 7**).

On the other hand, increased amounts of secosterol-B but not -A were formed when the PMA-activated nHL-60 cells and neutrophils isolated from WT mice were cultured in the medium containing 10% FBS (Figs. 2 and 4). Furthermore, higher levels of secosterol-B than -A were detected in the samples of plasma and liver collected from WT mice compared to those from MPO-deficient mice (Fig. 6). The secosterol-B levels were also significantly increased in the plasma samples of LPS-treated WT mice (Fig. 6). The origin of secosterol-B formed under these conditions is currently unknown, although there are two possibilities as described above: *a*) the conversion of secosterol-A to secosterol-B by aldolization (2, 10), and *b*) the direct formation of secosterol-B by the Hock-cleavage of 5α-hydroperoxy cholesterol (13, 14). On the basis of our results, the former pathway seems to be more important than any other. However, it is clear that under inflammatory conditions, increased amounts of secosterol-B could be formed and may exert adverse effects as discussed below.

It is widely accepted that oxysterols resulting from the chemical or enzymatic oxidation of cholesterol play pivotal roles in the development of cardiovascular diseases and atherosclerotic lesions (25–28). They might also be involved in the development of important degenerative diseases, such as Alzheimer's disease (29), osteoporosis (30–32), and age-related macular degeneration (32). In addition, it has been reported that secosterols induced apoptotic cell death at μM concentrations in several cultured cells, such as T- and B-cells, macrophage, cardiomyoblasts, and abdominal aortic endothelial cells (10, 19, 20). We also observed that secosterols are much more strongly cytotoxic (more than 10-fold) compared with five known toxic oxysterols, including 7β-hydroxycholesterol, 7-ketocholesterol, 5β,6β-epoxycholesterol, and 25-hydroxycholesterol for 48 h incubation in HL-60 cells (Tomono et al., unpublished observations). Further studies are warranted to elucidate the roles of cholesterol ozonolysis products, including their metabolites, in the development of atherosclerosis, neurodegenerative diseases, and other oxidative stress-related disorders, especially in the context of their reactions with tissue components, such as proteins, nucleic acids, and lipids, and their resulting effects on the biological functions of these components.

In conclusion, we demonstrated that secosterols are formed by PMA-activated human neutrophil-like cells as well as activated neutrophils obtained from WT mice. These activated neutrophils produce increased amounts of secosterol-A in the medium without 10% FBS, to which cholesterol was added exogenously. This secosterol-A formation was enhanced significantly by IgG, and the experiments with some enzyme inhibitors and scavengers of ROS imply that the reaction requires the generation of superoxide, hydrogen peroxide, hypochlorous acid, and singlet oxygen. On the basis of

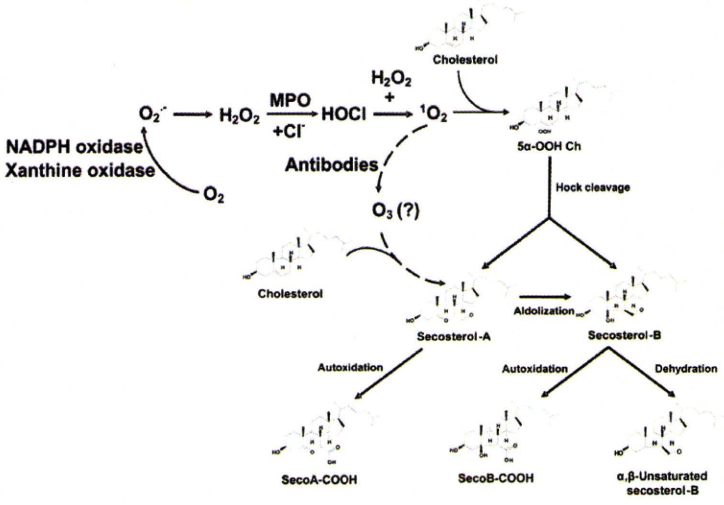

Fig. 7. Proposed mechanisms for the formation of secosterol-A, secosterol-B, and their oxidation products by activated neutrophils. α, β-unsaturated-secosterol-B, 3β-hydroxy-B-norcholest-5-ene; HOCl, hypochlorous acid; MPO, myeloperoxidase; secoA-COOH, 3β-hydroxy-5-oxo-secocholestan-6-oic acid; secoB-COOH, 3β-hydroxy-5β-hydroxy-B-norcholestane-6-oic acid; secosterol-A, 3β-hydroxy-5-oxo-5,6-secocholestan-6-al; secosterol-B, 3β-hydroxy-5β-hydroxy-B-norcholestane-6β-carboxaldehyde.

these findings, we conclude that secosterol-A, at least in the medium without 10% FBS, is formed by an ozone-like oxidant, which is generated by the catalysis of IgG in the presence of singlet oxygen and hydrogen peroxide. In addition, we clearly demonstrated that MPO plays an important role in the formation of secosterols. Possibly, hypochlorous acid generated by MPO is needed to generate singlet oxygen and, therefore, an ozone-like oxidant in the presence of hydrogen peroxide. As MPO has been implicated in the pathogenesis of atherosclerosis and neurodegenerative diseases, such as Alzheimer's disease (33, 34), further studies are needed to elucidate the biological roles of the MPO-mediated formation of secosterols and their further oxidation products in the development of these diseases.

The authors thank Yohei Wakao, Azusa Suzuki, Mina Yoshida, Kei Yamamoto, and Noriko Matsumoto for their technical support in animal experiments.

REFERENCES

1. Babior, B. M., C. Takeuchi, J. Ruedi, A. Gutierrez, and P. J. Wentworth. 2003. Investigating antibody-catalyzed ozone generation by human neutrophils. *Proc. Natl. Acad. Sci. USA.* **100:** 3031–3034.
2. Nieva, J., and P. J. Wentworth. 2004. The antibody-catalyzed water oxidation pathway–a new chemical arm to immune defense? *Trends Biochem. Sci.* **29:** 274–278.
3. Yamashita, K., T. Miyoshi, T. Arai, N. Endo, H. Itoh, K. Makino, K. Mizugishi, T. Uchiyama, and M. Sasada. 2008. Ozone production by amino acids contributes to killing of bacteria. *Proc. Natl. Acad. Sci. USA.* **105:** 16912–16917.
4. Kettle, A. J., B. M. Clark, and C. C. Winterbourn. 2004. Superoxide converts indigo carmine to isatin sulfonic acid: implications for the hypothesis that neutrophils produce ozone. *J. Biol. Chem.* **279:** 18521–18525.
5. Kettle, A. J., and C. C. Winterbourn. 2005. Do neutrophils produce ozone? An appraisal of current evidence. *Biofactors.* **24:** 41–45.
6. Gumulka, J., and L. L. Smith. 1983. Ozonization of cholesterol. *J. Am. Chem. Soc.* **105:** 1972–1979.
7. Jaworski, K., and L. L. Smith. 1988. Ozonization of cholesterol in nonparticipating solvents. *J. Org. Chem.* **53:** 545–554.
8. Paryzek, Z., J. Martynow, and W. Swoboda. 1990. The reaction of cholesterol with ozone and alcohols: a revised mechanism and structure of the principal product. *J. Chem. Soc., Perkin Trans.* **1:** 1222–1223.
9. Wentworth, A. D., B. D. Song, J. Nieva, A. Shafton, S. Tripurenani, and P. Wentworth, Jr. 2009. The ratio of cholesterol 5,6-secosterols formed from ozone and singlet oxygen offers insight into the oxidation of cholesterol in vivo. *Chem. Commun. (Camb.)* **(21):** 3098–3100.
10. Wentworth, P., Jr., J. Nieva, C. Takeuchi, R. Galve, A. D. Wentworth, R. B. Dilley, G. A. DeLaria, A. Saven, B. M. Babior, K. D. Janda, et al. 2003. Evidence for ozone formation in human atherosclerotic arteries. *Science.* **302:** 1053–1056.
11. Zhang, Q., E. T. Powers, J. Nieva, M. E. Huff, M. A. Dendle, J. Bieschke, C. G. Glabe, A. Eschenmoser, P. J. Wentworth, R. A. Lerner, et al. 2004. Metabolite-initiated protein misfolding may trigger Alzheimer's disease. *Proc. Natl. Acad. Sci. USA.* **101:** 4752–4757.
12. Bosco, D. A., D. M. Fowler, Q. Zhang, J. Nieva, E. T. Powers, P. J. Wentworth, R. A. Lerner, and J. W. Kelly. 2006. Elevated levels of oxidized cholesterol metabolites in Lewy body disease brains accelerate alpha-synuclein fibrilization. *Nat. Chem. Biol.* **2:** 249–253.
13. Brinkhorst, J., S. J. Nara, and D. A. Pratt. 2008. Hock cleavage of cholesterol 5alpha-hydroperoxide: an ozone-free pathway to the cholesterol ozonolysis products identified in arterial plaque and brain tissue. *J. Am. Chem. Soc.* **130:** 12224–12225.
14. Uemi, M., G. E. Ronsein, S. Miyamoto, M. H. G. Medeiros, and P. Di Mascio. 2009. Generation of cholesterol carboxyaldehyde by the reaction of singlet molecular oxygen [O2 (1Delta(g))] as well as ozone with cholesterol. *Chem. Res. Toxicol.* **22:** 875–884.
15. Tomono, S., N. Miyoshi, K. Sato, Y. Ohba, and H. Ohshima. 2009. Formation of cholesterol ozonolysis products through an ozone-free mechanism mediated by the myeloperoxidase-H_2O_2-chloride system. *Biochem. Biophys. Res. Commun.* **383:** 222–227.
16. Bieschke, J., Q. Zhang, E. T. Powers, R. A. Lerner, and J. W. Kelly. 2005. Oxidative metabolites accelerate Alzheimer's amyloidogenesis by a two-step mechanism, eliminating the requirement for nucleation. *Biochemistry.* **44:** 4977–4983.
17. Bieschke, J., Q. Zhang, D. A. Bosco, R. A. Lerner, E. T. Powers, P. J. Wentworth, and J. W. Kelly. 2006. Small molecule oxidation products trigger disease-associated protein misfolding. *Acc. Chem. Res.* **39:** 611–619.
18. Spillantini, M. G., and M. Goedert. 2000. The alpha-synucleinopathies: Parkinson's disease, dementia with Lewy bodies, and multiple system atrophy. *Ann. N. Y. Acad. Sci.* **920:** 16–27.
19. Sathishkumar, K., S. N. Murthy, and R. M. Uppu. 2007. Cytotoxic effects of oxysterols produced during ozonolysis of cholesterol in murine GT1–7 hypothalamic neurons. *Free Radic. Res.* **41:** 82–88.
20. Sathishkumar, K., M. Haque, T. E. Perumal, J. Francis, and R. M. Uppu. 2005. A major ozonation product of cholesterol, 3beta-hydroxy-5-oxo-5,6-secocholestan-6-al, induces apoptosis in H9c2 cardiomyoblasts. *FEBS Lett.* **579:** 6444–6450.
21. Collins, S. J., F. W. Ruscetti, R. E. Gallagher, and R. C. Gallo. 1978. Terminal differentiation of human promyelocytic leukemia cells

induced by dimethyl sulfoxide and other polar compounds. *Proc. Natl. Acad. Sci. USA.* **75:** 2458–2462.
22. Aratani, Y., H. Koyama, S. Nyui, K. Suzuki, F. Kura, and N. Maeda. 1999. Severe impairment in early host defense against Candida albicans in mice deficient in myeloperoxidase. *Infect. Immun.* **67:** 1828–1836.
23. Higashi, T., T. Ichikawa, S. Inagaki, J. Z. Min, T. Fukushima, and T. Toyo'oka. 2010. Simple and practical derivatization procedure for enhanced detection of carboxylic acids in liquid chromatography-electrospray ionization-tandem mass spectrometry. *J. Pharm. Biomed. Anal.* **52:** 809–818.
24. Stewart, C. R., L. M. Wilson, Q. Zhang, C. L. Pham, L. J. Waddington, M. K. Staples, D. Stapleton, J. W. Kelly, and G. J. Howlett. 2007. Oxidized cholesterol metabolites found in human atherosclerotic lesions promote apolipoprotein C–II amyloid fibril formation. *Biochemistry.* **46:** 5552–5561.
25. Bjorkhem, I., O. Andersson, U. Diczfalusy, B. Sevastik, R. J. Xiu, C. Duan, and E. Lund. 1994. Atherosclerosis and sterol 27-hydroxylase: evidence for a role of this enzyme in elimination of cholesterol from human macrophages. *Proc. Natl. Acad. Sci. USA.* **91:** 8592–8596.
26. Salonen, J. T., K. Nyyssonen, R. Salonen, E. Porkkala-Sarataho, T. P. Tuomainen, U. Diczfalusy, and I. Bjorkhem. 1997. Lipoprotein oxidation and progression of carotid atherosclerosis. *Circulation.* **95:** 840–845.
27. Brown, A. J., and W. Jessup. 1999. Oxysterols and atherosclerosis. *Atherosclerosis.* **142:** 1–28.
28. Larsson, D. A., S. Baird, J. D. Nyhalah, X-M. Yuan, and W. Li. 2006. Oxysterol mixtures, in atheroma-relevant proportions, display synergistic and proapoptotic effects. *Free Radic. Biol. Med.* **41:** 902–910.
29. Vaya, J., and H. M. Schipper. 2007. Oxysterols, cholesterol homeostasis, and Alzheimer disease. *J. Neurochem.* **102:** 1727–1737.
30. Kha, H. T., B. Basseri, D. Shouhed, J. Richardson, S. Tetradis, T. J. Hahn, and F. Parhami. 2004. Oxysterols regulate differentiation of mesenchymal stem cells: pro-bone and anti-fat. *J. Bone Miner. Res.* **19:** 830–840.
31. Shouhed, D., H. T. Kha, J. A. Richardson, C. M. Amantea, T. J. Hahn, and F. Parhami. 2005. Osteogenic oxysterols inhibit the adverse effects of oxidative stress on osteogenic differentiation of marrow stromal cells. *J. Cell. Biochem.* **95:** 1276–1283.
32. Liu, H., L. Yuan, S. Xu, K. Wang, and T. Zhang. 2005. Cholestane-3beta,5alpha,6beta-triol inhibits osteoblastic differentiation and promotes apoptosis of rat bone marrow stromal cells. *J. Cell. Biochem.* **96:** 198–208.
33. Nicholls, S. J., and S. L. Hazen. 2009. Myeloperoxidase, modified lipoproteins, and atherogenesis. *J. Lipid Res.* **50:** S346–S351.
34. Maki, R. A., V. A. Tyurin, R. C. Lyon, R. L. Hamilton, S. T. DeKosky, V. E. Kagan, and W. F. Reynolds. 2009. Aberrant expression of myeloperoxidase in astrocytes promotes phospholipid oxidation and memory deficits in a mouse model of Alzheimer disease. *J. Biol. Chem.* **284:** 3158–3169.

Abstract

OXIDATIVE STRESS-INDUCED TUMORIGENESIS IN THE SMALL INTESTINES OF DNA REPAIR-DEFICIENT MICE

Teruhisa Tsuzuki,* Jing Shu Piao,* Takuro Isoda,* Kunihiko Sakumi,† Yusaku Nakabeppu,† and Yoshimichi Nakatsu*

Oxygen radicals are produced through normal cellular metabolism, and the formation of such radicals is further enhanced by radiation and by various chemicals. Oxygen radicals attack DNA and its precursor nucleotides, and consequently bases with various modifications are introduced into the DNA of normally growing cells. One such modified base, 8-oxo-7, 8-dihydroguanine (8-oxoG) is highly mutagenic because of its ambiguous pairing property. Three enzymes, MTH1, OGG1, and MUTYH[1], play important roles in avoiding 8-oxoG-related mutagenesis in mammalian cells (Sekiguchi and Tsuzuki 2002; Sakumi et al. 2003; Tsuzuki et al. 2001, 2007).

The authors have established an experimental system for oxidative DNA damage-induced mutagenesis and tumorigenesis in the gastrointestinal tracts of mice (Sakamoto et al. 2007). Oral administration of an oxidizing reagent, potassium bromate ($KBrO_3$), effectively induced G:C to T:A transversions and epithelial tumors in the small intestines of *Mutyh*-deficient mice, implying the significance of Mutyh in the suppression of mutagenesis and tumorigenesis induced by oxidative stress. Mutation analyses were performed on the tumor-associated genes amplified from the intestinal tumors developed in four mutant mice that had been treated with $KBrO_3$. Many tumors had G:C to T:A transversions in either *Apc* or *Ctnnb1*. No mutations were found in either *K-ras* (exon 2) or *Trp53* (exon 5-8). These findings confirm the association between MUTYH-deficiency and the recessive form of hereditary multiple colorectal adenoma/carcinoma in humans, known as MUTYH-associated familial adenomatous polyposis (Al-Tassan et al. 2002), with the characteristic feature: G:C to T:A transversions in the GAA sequence context. Also, these results suggest that the abnormality in the Wnt signal transduction pathway is causatively associated with oxidative stress-induced tumorigenesis in the small intestines of *Mutyh*-deficient mice. In addition, the multiple formation of tumors in the small intestines of *Mutyh*-deficient mice provides a suitable model system to investigate the processes of intestinal tumorigenesis.[2]

Xie et al. showed that *Mutyh/Ogg1* double-deficient mice predominantly developed lung and ovarian tumors as well as lymphomas (Xie et al. 2004). They also showed that 8.6% of *Mutyh/Ogg1* double-deficient mice exhibited adenomas/carcinomas in their gastrointestinal tracts, which were not observed in wild-type mice. The current researchers and other groups have previously reported that there was little difference in the number of intestinal tumors in wild-type and Ogg1-null mice, although an Ogg1 deficiency resulted in 8-oxoG buildup in genomic DNA and an elevated mutation frequency in the latter (Klungland et al. 1999; Minowa et al. 2000; Sakumi et al. 2003). Thus, the development of intestinal tumors in *Mutyh/Ogg1* double-deficient mice supports the notion that having a Mutyh deficiency does indeed increase susceptibility to intestinal tumorigenesis regardless of the genetic background or environmental factors.

It is of interest that the deficiency of Mutyh but not Ogg1 makes mice susceptible to intestinal tumorigenesis, although the deficiency of either Mutyh or Ogg1 increases G:C to T:A transversion at almost equal frequency in the small intestines of mice. It is possible that this difference may be attributed to the additional substrate; MUTYH excises 2-hydroxyadenine, an oxidized adenine, paired with guanine, beside adenine paired with 8-oxoguanine, from DNA (Ohtusbo et al. 2000; Ushijima et al. 2005). However, Oka et al. recently reported the involvement of Mutyh in cell death caused by oxidative

[1]MUTYH - human protein in print, or gene in italic; Mutyh - mouse counterparts, respectively.

* Department of Medical Biophysics and Radiation Biology, Faculty of Medical Sciences; † Division of Neurofunctional Genomics, Medical Institute of Bioregulation, Kyushu University, Fukuoka, 812-8582 Japan.

For correspondence contact: T. Tsuzuki, Department of Medical Biophysics and Radiation Biology, Faculty of Medical Sciences, Kyushu University, Fukuoka, 812-8582 Japan, or email at tsuzuki@med.kyushu-u.ac.jp.

(*Manuscript accepted* 2 *June* 2010)
0017-9078/10/0

DOI: 10.1097/HP.0b013e3181eaf2c7

[2]Isoda et al., in preparation.

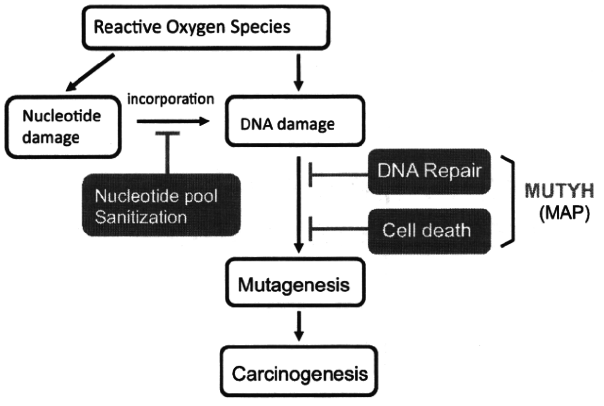

Fig. 1. The roles of MUTYH in the avoiding mechanisms for ROS-induced mutagenesis and carcinogenesis. The defect in Mutyh simultaneously compromises both DNA repair and cell-death induced by oxidative DNA damage. Thus, the defect in Mutyh makes mice highly susceptible to oxidative stress-induced tumorigenesis. This may provide molecular bases for explaining why among the factors involved in suppressing oxidative damage-induced mutagenesis, only MUTYH is, so far, identified to be associated with hereditary colorectal cancers in humans.

DNA damage (Oka et al. 2008). Thus, the defect in Mutyh would simultaneously compromise both DNA repair and cell-death induced by oxidative DNA damage (Fig. 1). This may explain why among the factors involved in suppressing oxidative damage-induced mutagenesis only MUTYH is, so far, identified to be associated with hereditary colorectal cancers in humans.

Acknowledgments—A part of this text is adopted from Extended Abstracts for the 40th International Symposium of the Princess Takamatsu Cancer Research Fund: DNA Repair and Human Cancers, held in November 10–12, 2009, Tokyo, Japan. Health Phys. 100(3):293–294; 2011

Key words: carcinogenesis; mice; radiation, biology; tumors

REFERENCES

Al-Tassan N, Chmiel NH, Maynard J, Fleming N, Livingston AL, Williams GT, Hodges AK, Davies DR, David SS, Sampson JR, Cheadle JP. Inherited variants of MYH associated with somatic G:C to T:A mutations in colorectal tumors. Nat Genet 30:227–232; 2002.

Klungland A, Rosewell I, Hollenbach S, Larsen E, Daly G, Epe B, Seeberg E, Lindahl T, Barnes DE. Accumulation of premutagenic DNA lesions in mice defective in removal of oxidative base damage. Proc Natl Acad Sci USA 96:13300–13305; 1999.

Minowa O, Arai T, Hirano M, Monden Y, Nakai S, Fukuda M, Itoh M, Takano H, Hippou Y, Aburatani H, Masumura K, Nohmi T, Nishimura S, Noda T. *Mmh/Ogg1* gene inactivation results in accumulation of 8-hydroxyguanine in mice. Proc Natl Acad Sci USA 97:4156–4161; 2000.

Ohtsubo T, Nishioka K, Imaiso Y, Iwai S, Shimokawa H, Oda H, Fujiwara T, Nakabeppu Y. Identification of human MutY homolog (hMYH) as a repair enzyme for 2-hydroxyadenine in DNA and detection of multiple forms of hMYH located in nuclei and mitochondria. Nucleic Acids Res 28:1355–1364; 2000.

Oka S, Ohno M, Tsuchimoto D, Sakumi K, Furuichi M, Nakabeppu Y. Two distinct pathways of cell death triggered by oxidative damage to nuclear and mitochondrial DNAs. EMBO J 27:421–432; 2008.

Sakamoto K, Tominaga Y, Yamauchi K, Nakatsu Y, Sakumi K, Yoshiyama K, Egashira A, Kura S, Yao T, Tsuneyoshi M, Maki H, Nakabeppu Y, Tsuzuki T. MUTYH-null mice are susceptible to spontaneous and oxidative stress-induced intestinal tumorigenesis. Cancer Res 67:6599–6604; 2007.

Sakumi K, Tominaga Y, Furuichi M, Xu P, Tsuzuki T, Sekiguchi M, Nakabeppu Y. OGG1 knockout-associated lung tumorigenesis and its suppression by Mth1 gene disruption. Cancer Res 63:902–905; 2003.

Sekiguchi M, Tsuzuki T. Oxidative nucleotide damage: consequences and prevention. Oncogene 21:8895–8904; 2002.

Tsuzuki T, Egashira A, Igarashi H, Iwakuma T, Nakatsuru Y, Tominaga Y, Kawate H, Nakao K, Nakamura K, Ide F, Kura S, Nakabeppu Y, Katsuki M, Ishikawa T, Sekiguchi M. Spontaneous tumorigenesis in mice defective in the MTH1 gene encoding 8-oxo-dGTPase. Proc Natl Acad Sci USA 98:11456–1146; 2001.

Tsuzuki T, Nakatsu Y, Nakabeppu Y. Significance of error-avoiding mechanisms for oxidative DNA damage in carcinogenesis. Cancer Sci 98:465–470; 2007.

Ushijima Y, Tominaga Y, Miura T, Tsuchimoto D, Sakumi K, Nakabeppu Y. A functional analysis of the DNA glycosylase activity of mouse MUTYH protein excising 2-hydroxyadenine opposite guanine in DNA. Nucleic Acids Res 33(2):672–682; 2005.

Xie Y, Yang H, Cunanan C, Okamoto K, Shibata D, Pan J, Barnes DE, Lindahl T, McIlhatton M, Fishel R, Miller JH. Deficiencies in mouse *MYH* and *OGG1* result in tumor predisposition and G to T mutations in codon 12 of the K-ras oncogene in lung tumors. Cancer Res 64:3096–3092; 2004.

THE JOURNAL OF BIOLOGICAL CHEMISTRY VOL. 285, NO. 1, pp. 444–452, January 1, 2010

Structural and Dynamic Features of the MutT Protein in the Recognition of Nucleotides with the Mutagenic 8-Oxoguanine Base*[S]

Received for publication, September 15, 2009, and in revised form, October 14, 2009 Published, JBC Papers in Press, October 28, 2009, DOI 10.1074/jbc.M109.066373

Teruya Nakamura[‡], Sachiko Meshitsuka[§], Seiju Kitagawa[§], Nanase Abe[§], Junichi Yamada[§], Tetsuya Ishino[§], Hiroaki Nakano[§], Teruhisa Tsuzuki[¶], Takefumi Doi[§], Yuji Kobayashi[§], Satoshi Fujii[‖], Mutsuo Sekiguchi[**], and Yuriko Yamagata[‡1]

From the [‡]Graduate School of Pharmaceutical Sciences, Kumamoto University, Kumamoto 862-0973, the [§]Graduate School of Pharmaceutical Sciences, Osaka University, Suita 565-0871, the [¶]Graduate School of Medical Sciences, Kyushu University, Fukuoka 812-8582, the [‖]School of Pharmaceutical Sciences, University of Shizuoka, Shizuoka 422-8526, and the [**]Fukuoka Dental College, Fukuoka 814-0193, Japan

Escherichia coli **MutT hydrolyzes 8-oxo-dGTP to 8-oxo-dGMP, an event that can prevent the misincorporation of 8-oxoguanine opposite adenine in DNA. Of the several enzymes that recognize 8-oxoguanine, MutT exhibits high substrate specificity for 8-oxoguanine nucleotides; however, the structural basis for this specificity is unknown. The crystal structures of MutT in the apo and holo forms and in the binary and ternary forms complexed with the product 8-oxo-dGMP and 8-oxo-dGMP plus Mn^{2+}, respectively, were determined. MutT strictly recognizes the overall conformation of 8-oxo-dGMP through a number of hydrogen bonds. This recognition mode revealed that 8-oxoguanine nucleotides are discriminated from guanine nucleotides by not only the hydrogen bond between the N7-H and Oδ (N119) atoms but also by the *syn* glycosidic conformation that 8-oxoguanine nucleotides prefer. Nevertheless, these discrimination factors cannot by themselves explain the roughly 34,000-fold difference between the affinity of MutT for 8-oxo-dGMP and dGMP. When the binary complex of MutT with 8-oxo-dGMP is compared with the ligand-free form, ordering and considerable movement of the flexible loops surrounding 8-oxo-dGMP in the binary complex are observed. These results indicate that MutT specifically recognizes 8-oxoguanine nucleotides by the ligand-induced conformational change.**

Although spontaneous mutations are indispensable to the evolutionary process of living organisms, they can also be lethal to the organism. Among the various modified bases in DNA, RNA, and nucleotides, 8-oxoguanine (8-oxoG),[2] a damaged form of guanine (G) generated by reactive oxygen species, is known to have highly mutagenic potency because of its mispairing with adenine. Therefore, organisms have an error avoidance pathway for preventing mutations caused by 8-oxoG. The *Escherichia coli* MutT protein (129 amino acids, M_r = 14,900) hydrolyzes 8-oxo-dGTP and 8-oxo-GTP to their corresponding nucleoside monophosphates and inorganic pyrophosphate in the presence of Mg^{2+} (1, 2). Because 8-oxo-dGTP and 8-oxo-GTP can be misincorporated opposite adenine by DNA and RNA polymerases, the hydrolysis of the damaged nucleotides by MutT can avoid replicational and transcriptional errors. In DNA, 8-oxoG paired with cytosine is excised by MutM, an 8-oxoG DNA glycosylase, whereas MutY, an adenine DNA glycosylase, removes adenine paired with 8-oxoG (3–6).

The substrate specificities of enzymes that recognize 8-oxoG are quite varied. MutT exhibits high substrate specificity for 8-oxoG nucleotides; that is, the K_m for 8-oxo-dGTP is 14,000-fold lower than that for dGTP (7). In contrast, human MutT homologue 1 (hMTH1) hydrolyzes not only 8-oxo-dGTP but also several oxidized purine nucleotides such as 2-oxo-dATP, 2-oxo-ATP, 8-oxo-dATP, and 8-oxo-ATP. In terms of the hydrolysis of 8-oxo-dGTP, the K_m of hMTH1 for 8-oxo-dGTP is only 17-fold lower than that for dGTP (8, 9). The solution structure of hMTH1 as determined by NMR has revealed its overall architecture and possible substrate-binding region (10); however, the broad substrate recognition mechanism of hMTH1 remains to be elucidated. MutM and MutY also have low specificity for 8-oxoG. For example, MutM can recognize a variety of damaged bases such as formamidopyrimidine, 5-hydroxycytosine, and dihydrouracil in addition to 8-oxoG (11–13), and MutY shows a kinetic preference for A:8-oxoG that is only 6-fold greater than that for A:G (14).

The crystal structures of OGG1, MutM, and MutY complexed with 8-oxoG-containing DNA (13, 15, 16) have revealed

* This work was supported in part by grants-in-aid for scientific research and the National Project for Protein Structural and Functional Analysis from the Ministry of Education, Culture, Sports, Sciences and Technology of Japan.

[S] The on-line version of this article (available at http://www.jbc.org) contains supplemental Figs. S1–S4.

The atomic coordinates and structure factors (codes 3A6S, 3A6T, 3A6U, and 3A6V) have been deposited in the Protein Data Bank, Research Collaboratory for Structural Bioinformatics, Rutgers University, New Brunswick, NJ (http://www.rcsb.org/).

[1] To whom correspondence should be addressed: Graduate School of Pharmaceutical Sciences, Kumamoto University, 5-1 Oe-honmachi, Kumamoto 862-0973, Japan. Tel./Fax: 81-96-371-4638; E-mail: yamagata@gpo.kumamoto-u.ac.jp.

[2] The abbreviations used are: 8-oxoG, 8-oxoguanine; Nudix, nucleoside diphosphate linked to some other moiety, X; SLHL, strand-loop-helix-loop; r.m.s.d., root mean square deviation; AMPCPP, adenosine 5′-(α,β-methyleneltriphosphate); SeMet, selenomethionine; hMTH1, human MutT homologue 1.

that, interestingly, OGG1 and MutM do not recognize the O8 atom, which is the most characteristic feature of the 8-oxoG moiety, and the interaction observed between the O8 atom and the main-chain atom of MutY is relatively weak. Alternatively, OGG1, MutM, and MutY commonly discriminate 8-oxoG from G by the protonation at N7 accompanied by the oxidation of C8. Structural studies on various enzymes that recognize 8-oxoG have succeeded in explaining the mechanism by which 8-oxoG is discriminated from normal G in DNA, but one of the most interesting questions to be elucidated is the mechanism by which MutT acquires extremely high substrate specificity for 8-oxoG compared with the other enzymes.

MutT belongs to the Nudix (nucleoside diphosphate linked to some other moiety, X) hydrolase family (17). Nudix family members have a highly conserved MutT signature (Nudix motif); *i.e.* $GX_5EX_7REUXEEXGU$, where U is a hydrophobic residue and X is any amino acid. Current genome analyses have found a large number of open reading frames containing the MutT signature, but their functions, *i.e.* their substrates, are not identified in the case of almost all these proteins because of a lack of homology outside the MutT signature. MutT is the most examined protein in this family. Its structure was first determined by NMR (18) and has greatly contributed to the study of the Nudix hydrolase family. NMR studies of MutT with its product, 8-oxo-dGMP, have predicted several recognition models of 8-oxo-dGMP (19). However, the precise recognition mechanism of 8-oxoG nucleotides remains unclear. Therefore, it is necessary to determine the crystal structures of MutT to explain the extremely high substrate specificity of MutT for 8-oxoG nucleotides.

Here, we present x-ray crystallographic analyses of the apo enzyme; the Mn^{2+}-bound holo enzyme (MutT-Mn^{2+}); the binary complex with 8-oxo-dGMP, a reaction product (MutT-8-oxo-dGMP); and the tertiary complex with 8-oxo-dGMP and Mn^{2+} (MutT-8-oxo-dGMP-Mn^{2+}). These structures have revealed the mechanism of the extremely high substrate specificity of MutT for 8-oxoG nucleotides and have allowed us to propose the exact roles of some conserved residues in the MutT signature.

EXPERIMENTAL PROCEDURES

Protein Expression and Purification—The *E. coli* strain BL21 (DE3) harboring a newly constructed pET8c/MutT plasmid was used for the expression of native and selenomethionine (SeMet)-substituted MutTs. Native MutT was overexpressed in Luria-Bertani (LB) broth, and SeMet MutT was overexpressed in LeMaster broth containing seleno-DL-methionine instead of methionine with sufficient amounts of isoleucine, lysine, and threonine to inhibit the methionine pathway (20, 21). This condition was also present in the overexpression of SeMet hMTH1 (22). Purification of MutT was carried out by almost the same procedure (except that the hydroxyapatite column chromatography step was skipped), as described previously (23). DEAE-Sepharose and the HiPrep 16/60 Sephacryl S-200 HR column were substituted for DEAE-Sephacel and the Sephadex G-75 column, respectively. The purified protein solution was concentrated to ~6 mg/ml.

Crystallization—The native and SeMet-substituted apo forms and all complexes were crystallized by hanging drop vapor diffusion at 288 K. Crystals of native and SeMet-substituted forms were obtained from a droplet containing 3 mg/ml protein, 10 mM Tris-HCl (pH 7.5), 0.5 mM EDTA, 2.5% glycerol, 0.5 mM 2-mercaptoethanol, 0.7 M potassium sodium tartrate, and 44 mM HEPES-NaOH (pH 7.5) equilibrated against a reservoir containing 1.4 M potassium sodium tartrate and 87 mM HEPES-NaOH (pH 7.5). Crystals of MutT-Mn^{2+} were obtained in the same manner, as described above, except that 10 mM $MnCl_2$ was added to the droplet. The crystallizations of MutT-8-oxo-dGMP and MutT-8-oxo-dGMP-Mn^{2+} were described previously (24). The crystals were transferred to a cryosolution of each reservoir containing 30% sucrose and were then flash frozen.

Data Collection, Processing, Phasing, and Structure Refinement—Diffraction data were collected at 100 K on beamline 18B of the Photon Factory (Tsukuba, Japan) and on beamlines 41XU, 44XU, 38B1, and 40B2 of SPring-8 (Harima, Japan). The data for native and SeMet derivative forms were processed and scaled by DSP/MOSFLM and SCALA (25). The data for MutT-Mn^{2+} were processed and scaled by DENZO and SCALEPACK (26). There are two molecules in the asymmetric unit with V_M of 2.2 (native MutT) and 2.5 (MutT-Mn^{2+}) $Å^3 \cdot Da^{-1}$ (27). Data collection statistics of the best data used for structure determination and refinements are listed in Table 1. Data collection statistics of MutT-8-oxo-dGMP and MutT-8-oxo-dGMP-Mn^{2+} are quoted from the reference by Nakamura *et al.* (24).

The positions of eight selenium atoms were determined using SOLVE (28). The initial phases were calculated using MLPHARE (29) and improved using DM (30). The initial model was built using TOM (31) and O (32). The model was refined using X-PLOR (33) and CNS (34). Using the model of the SeMet derivative, the successive refinement of native MutT converged at an R value of 20.4% and an R_{free} of 23.1% for reflections in the resolution range 20–1.8 Å. The structure of MutT-8-oxo-dGMP was solved by molecular replacement with AMoRe (35) using the structure of the native apo form as a search model. The $2F_o - F_c$ maps after CNS refinements clearly showed the density for 8-oxo-dGMP and the conformationally changed loop regions (L-A and L-D). These regions were manually built and fitted into the density with O. The structure of MutT-8-oxo-dGMP-Mn^{2+} was refined starting with the coordinates of the MutT-8-oxo-dGMP. The structure of MutT-Mn^{2+} was solved by molecular replacement with AMoRe by using the structure of the apo form as a search model. The stereochemical qualities of the structures were checked by PROCHECK (36); the refinement statistics are listed in Table 2. Superposition of MutT structures were carried out using Lsqkab (37). All molecular graphics were prepared using PyMOL (38).

RESULTS AND DISCUSSION

Overall Structures of MutT and MutT-8-oxo-dGMP—The crystal structures of the MutT apo and MutT-8-oxo-dGMP complex forms were determined at a resolution of 1.8 and 1.96 Å, respectively. MutT is composed of two α-helices (α-1 and α-2) and six β-strands (β-1 to β-6) (Figs. 1 and 2*A*); it adopts an

TABLE 1

Data collection statistics

Values in parentheses correspond to the highest resolution shell.

Diffraction data	MutT				MutT–8-oxo-dGMP	MutT–8-oxo-dGMP–Mn^{2+}
	Native	Peak	Edge	Remote		
Beam line	SPring-8 BL41XU		PF BL18B		SPring-8 BL41XU	SPring-8 BL40B2
Wavelength (Å)	0.7080	0.9793	0.9791	0.9500	0.9000	1.296
Space group	$P2_1$		$P2_1$		$P2_12_12_1$	$P2_12_12_1$
Unit-cell lengths (Å, °)	$a = 33.9$		$a = 34.1$		$a = 37.9$	$a = 38.2$
	$b = 71.6$		$b = 71.1$		$b = 56.0$	$b = 56.0$
	$c = 55.8$		$c = 55.7$		$c = 59.4$	$c = 59.3$
	$\beta = 99.0$		$\beta = 98.7$			
Resolution range (Å)	20.0–1.8 (1.9–1.8)		20.0–2.2 (2.3–2.2)		20.0–1.96 (2.08–1.96)	18.56–2.56 (2.72–2.56)
No. of observed reflections	85,618	49,308	49,226	50,094	54,195	26,502
No. of unique reflections	24,217	13,041	13,015	13,147	9,344	4,395
Completeness (%)	99.7 (99.7)	97.2 (97.2)	97.3 (97.3)	98.3 (98.3)	97.6 (93.2)	99.2 (95.7)
R_{merge}[a] (%)	3.1 (9.4)	3.9 (12.1)	3.8 (12.3)	3.9 (12.1)	6.5 (18.1)	7.7 (15.2)
$\langle I/\sigma \rangle$	15.8 (7.9)	8.8 (3.3)	9.4 (5.0)	8.8 (5.6)	29.6 (6.2)	45.9 (22.6)

	MutT-Mn^{2+}
Beam line	PF BL18B
Wavelength (Å)	1.000
Space group	$P2_1$
Unit-cell lengths (Å, °)	$a = 35.8$
	$b = 56.0$
	$c = 74.1$
	$\beta = 96.4$
Resolution range (Å)	40.0–2.0 (2.03–2.00)
No. of observed reflections	77,213
No. of unique reflections	19,810
Completeness (%)	98.1 (96.2)
R_{merge}[a] (%)	4.2 (6.4)
$\langle I/\sigma \rangle$	28.6 (18.6)

[a] $R_{merge} = 100 \times \Sigma|I_{hkl} - \langle I_{hkl} \rangle|/\Sigma I_{hkl}$, $\langle I_{hkl} \rangle$ is the mean value of I_{hkl}.

TABLE 2

Refinement statistics

Diffraction data	MutT	MutT–8-oxo-dGMP	MutT–8-oxo-dGMP–Mn^{2+}	MutT-Mn^{2+}
Resolution range (Å)	20.0–1.8	20.0–1.96	18.56–2.56	20.0–2.0
Number of reflections used	24,213	9,280	4,394	19,386
Number of atoms				
Protein	2,025	1,038	1,029	2,010
Water	190	136	92	131
Nucleotide	0	24	24	0
Mn^{2+} ion	0	0	1	4[a]
Other	11	34	5	32
Completeness (%)	99.1	97.3	99.9	98.1
R_{cryst}/R_{free}[b] (%)	20.4/23.1	17.8/20.1	19.3/24.2	19.2/22.7
Ramachandran plot (%)				
Most favored	93.0	91.5	87.6	94.9
Additional allowed	7.0	8.5	12.4	5.1
Generously allowed	0	0	0	0
Disallowed	0	0	0	0
r.m.s.d. in bonds (Å)	0.005	0.005	0.007	0.005
r.m.s.d. in angles (°)	1.2	1.3	1.3	1.2

[a] Two ions per monomer.

[b] $R_{cryst} = 100 \times \Sigma||F_o| - |F_c||/\Sigma|F_o|$. R_{free} was calculated from the test set (5% of the total data).

α-β-α sandwich structure that is conserved among members of the Nudix family. The Nudix motif (23 residues from Gly-38 *i.e.* the MutT signature ($GX_5EX_7REUXEEXGU$), adopts the characteristic strand-loop-helix-loop (SLHL) structure formed by β-3′, L-B, α-1, and L-C (39, 40). The crystal of the apo form contains two protein molecules per asymmetric unit, and they are very similar to each other with root mean square deviation (r.m.s.d.) of 0.5 Å for the corresponding 121 Cα atoms. For simplicity, only one molecule will be referred to in all further discussions. MutT exists as a monomer, which is found in the MutT-8-oxo-dGMP crystal.

In the apo form, the electron densities of L-A connecting β-2 and β-3 are not available, indicating that the L-A loop region has a highly flexible conformation (Fig. 2*A*). On the other hand, in the MutT-8-oxo-dGMP complex, the ordering of the flexible L-A loop by interactions with 8-oxo-dGMP was observed (Fig. 2, *B* and *C*). The plot of the displacement between the Cα atoms of the apo and complex forms is shown in supplemental Fig. S1*A*. The movements of the L-A and L-D regions are large (~8–10 Å) (Fig. 2*C* and supplemental Fig. S1*A*). Except for these loop regions, the two forms have a similar structure with an r.m.s.d. of 0.9 Å for the corresponding 101 Cα atoms.

A structural similarity search performed using the DALI server (41), with the coordinates of MutT-8-oxo-dGMP, indicated that 62 proteins (154 Protein Data Bank (PDB) ID numbers, 278 protein chains) are structural homologs of MutT with Z-scores of >6.0 and belong to the Nudix superfamily with the Nudix fold. The MutT structure, with two α-helices and six β-strands, comprises the smallest structural unit among members of the Nudix superfamily. Of 62 proteins, half have

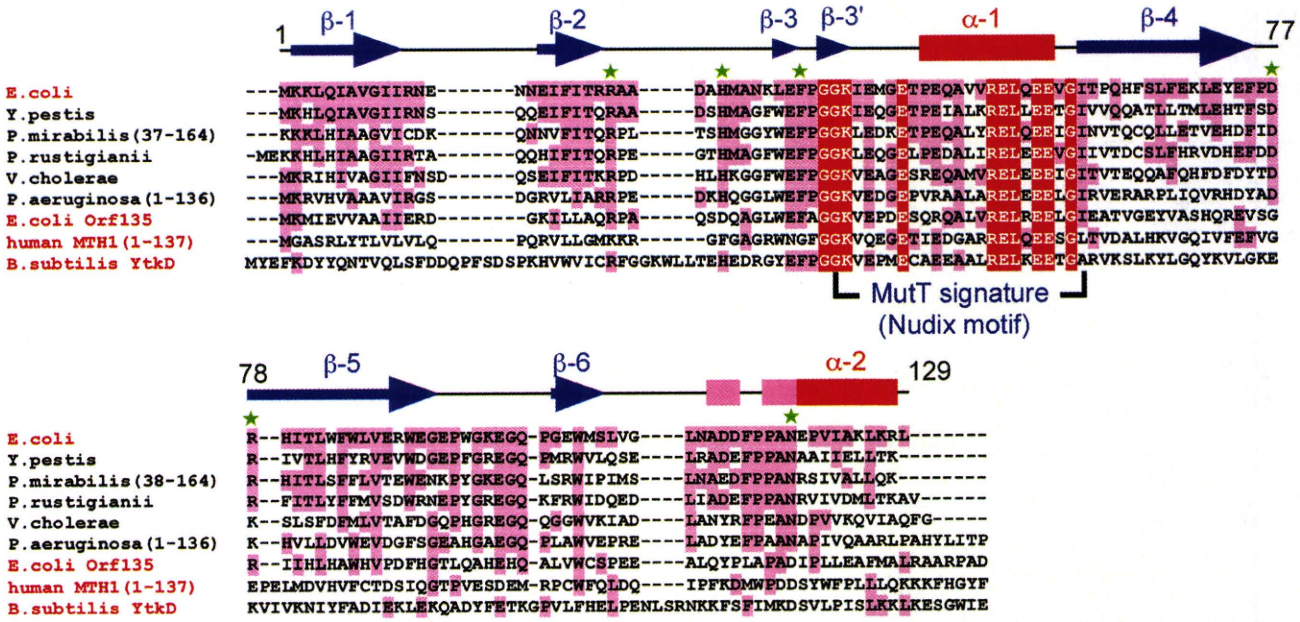

FIGURE 1. **Sequence alignment of MutT family proteins.** Amino acid sequences of MutT family proteins were aligned using ClustalW (72). MutT homologs from species related to *E. coli*, which share high sequence similarity, were chosen and are listed. They are from *E. coli* (CAA28523), *Yersinia pestis* (NP_670913), *Proteus mirabilis* (ZP_03840798), *Providencia rustigianii* (ZP_03315124), *Vibrio cholerae* (NP_232022), and *Pseudomonas aeruginosa* (ZP_04932260). In addition to *E. coli* MutT, *E. coli* Orf135 (BAA15549), human MTH1 (BAA07601), and *B. subtilis* YtkD (NP_390941), which have 8-oxo-dGTPase activity *in vitro*, were added and are shown in *red*. Absolutely conserved residues are shown in *red*, and identical residues are in *pink*. The *green asterisks* on the *E. coli* MutT sequence indicate amino residues that participate in the recognition of 8-oxoG and the ligand-induced conformational change. The secondary structure of *E. coli* MutT in the apo form is shown at the *top*. The α-helices, β-strands, and 3_{10} helices are represented as *red bars*, *blue arrows*, and *pink bars*, respectively.

unknown functions. Structures that are highly similar to the MutT complex form are the monomer structures of *Bdellovibrio bacteriovorus* RNA pyrophosphohydrolase; *i.e.* BdRppH in the ternary and binary forms complexed with GTP and Mg^{2+} (BdRppH-GTP-Mg^{2+}, 3FFU, r.m.s.d. = 1.8 Å, Z = 19.0) and with dGTP (BdRppH-dGTP, 3EF5, r.m.s.d. = 1.9 Å, Z = 18.3) (40) and unknown proteins from *Bartonella henselae* (3HHJ, r.m.s.d. = 1.8 Å, Z = 19.8) and *Methanosarcina mazei* (3GRN, r.m.s.d. = 2.1 Å, Z = 17.5), respectively. In MutT, the r.m.s.d. is rather large: 3.3 Å for 120 Cα atoms between the x-ray and NMR structures in the ligand-free form and 3.5 Å for 127 Cα atoms between structures in the complex form (PDB IDs: 1MUT and 1PUS) (18, 19).

Recognition Scheme of 8-oxo-dGMP by MutT—When 8-oxo-dGMP binds to MutT, large ligand-induced conformational changes occur in the L-A and L-D regions, namely, the ordering of the flexible L-A loop and considerable movement of L-A and L-D to the surrounding 8-oxo-dGMP (Figs. 2*C* and 3*A*). The side chains of Arg-23 and His-28 on L-A form hydrogen-bonding interactions with phosphate and sugar moieties of 8-oxo-dGMP, respectively, whereas Arg-78 interacts with the sugar moiety through a water-mediated hydrogen bond. Asp-77 and Arg-78 make two hydrogen bonds between their side chains. The conformational change of the L-A and L-D regions also produces the water molecule-mediated interaction between His-28 and Asp-77 and the CH-π interaction between His-28 and Phe-75 (Fig. 3*A* and supplemental Fig. S2). Thus, the loops L-A and L-D connect to each other, resulting in the formation of a cave composed of β-1, β-3, β-3′, β-5, and α-2 for substrate binding (Fig. 3*B*). 8-Oxo-dGMP is inserted deeply into the cave in which the wall on one side is filled with hydrophobic residues (Leu-4, Ile-6, Val-8, Ile-80, and Leu-82), and the other side and bottom include some polar residues (Arg-23 and Asn-119). The 8-oxoG base and the deoxyribose are perfectly buried, and the phosphate group faces the solvents (Fig. 3*B*). The glycosidic conformation of 8-oxo-dGMP bound to MutT is *syn*. This fact is consistent with the first suggestion by Bessman *et al.* that MutT may recognize the *syn* conformation, because the 8-substituted purine nucleotides were better substrates compared with the normal purine nucleotides (42). The sugar ring puckering and the sugar-phosphate backbone conformation of 8-oxo-dGMP are C2′-*endo* and *gauche*$^-$-*trans*, respectively. These conformations are generally observed in 8-substituted purine nucleosides and 5′-nucleotides (43).

These ligand-induced conformational changes result in the strict recognition of the overall structure of 8-oxo-dGMP by MutT through a number of hydrogen bonds (Fig. 3*C*). The characteristic features of the 8-oxoG base are the oxygen atom (O8) at C8 and the hydrogen atom (N7-H) at N7 accompanied by oxidation. MutT recognizes N7-H of 8-oxoG by a hydrogen bond with Oδ of Asn-119 (Fig. 3*C*, a *red dashed line*). The 8-oxoG base is also recognized by hydrogen bonds with Asn-119 and Phe-35; *i.e.* the Nδ of Asn-119 forms a hydrogen bond with O6 of 8-oxoG, and the main-chain atoms of Phe-35 participate in three types of hydrogen bonds with N2-H, N1-H, and O6. On the other hand, the O8 atom does not form hydrogen bonds with any amino acid residues, although it does participate in the weak C-H–O interaction with the phenyl ring C-H of Phe-75 (C–O distance, 3.4 Å) and the van der Waals interactions with the side-chain C-H moieties of Phe-75, Pro-116, Leu-

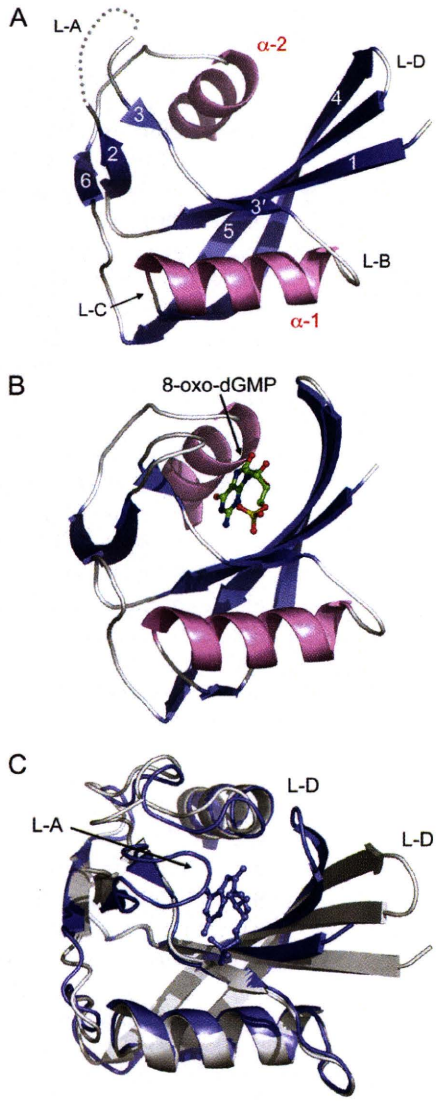

FIGURE 2. **Crystal structures of MutT apo and MutT-8-oxo-dGMP complex forms.** *A*, overall structure of MutT. α-Helices are in *pink*, and β-strands are in *slate*. A missing region of L-A is shown as a *gray dashed line*. *B*, overall structure of MutT-8-oxo-dGMP. 8-Oxo-dGMP is shown in *ball and stick representation*. *C*, comparison of the structures of the apo and complex forms. Apo and complex forms are shown in *gray* and *slate*, respectively. L-A and L-D regions in MutT-8-oxo-dGMP adopt a closed conformation as compared with those in the apo form.

82, Ile-80, and Ala-118 (Fig. 3*D*). In addition, the carbonyl oxygen of Gly-37 forms water molecule-mediated hydrogen bonds with N2-H of 8-oxoG and the phosphate oxygen. The side chain of His-28 is directly hydrogen-bonded to the O3′ atom of the deoxyribose. The O3′ atom also forms a hydrogen bond with a water molecule, binding to the side chain of Arg-78. The phosphate group forms a hydrogen bond with the side chain of Arg-23 and a water molecule-mediated hydrogen bond with the main chain of Lys-39. In summary, 8-oxo-dGMP is surrounded by 12 types of hydrogen bonds. The hydrogen-bonding interactions with the pyrimidine moiety and the α-phosphate group in MutT-8-oxo-dGMP are similar to those with the corresponding pyrimidine moieties and α-phosphate groups in the structures of BdRppH-GTP-Mg^{2+} and BdRppH-dGTP (BdRppH-(d)GTPs) (40). The positions of the base moieties of (d)GTPs with the *syn* conformation in BdRppH-(d)GTPs accord with that of 8-oxo-dGMP in MutT-8-oxo-dGMP with an r.m.s.d. of 0.6 Å for the corresponding 11 atoms when proteins are superimposed. BdRppH with Arg-40, Phe-52, and Asn-136 residues corresponding to Arg-23, Phe-35, and Asn-119 of MutT, respectively, recognizes N1-H, N2-H, and O6 of the pyrimidine moiety by four hydrogen bonds with Phe-52 and Asn-136; Pα-O of the α-phosphate group is recognized by a hydrogen bond with Arg-40. This recognition mode is the same as that observed in MutT. Apart from the similarities, differences are found in recognition of the imidazole moiety of the base and the sugar moiety as well as in the ligand-induced conformational change. The imidazole and sugar moieties of (d)GTPs in BdRppH-(d)GTPs do not form hydrogen bonds with any residues in BdRppH. In addition, although ligand-induced conformational change with loop ordering is observed in BdRppH, the change is significantly small (~2–4 Å) as compared with that in MutT. The large ligand-induced conformational change observed in MutT does contribute to its high affinity for 8-oxoG nucleotides, as discussed below. There is a large discrepancy between the K_m values of 0.081 and 268 μM for the hydrolysis of 8-oxo-dGTP by MutT and of dGTP by BdRppH, respectively (7, 44). This may derive from these structural differences, in addition to the unfavorable *syn* conformation of (d)GTPs in BdRppH-(d)GTPs.

As a result of the strict recognition of 8-oxo-dGMP with the large conformational change, there are low *B* factors and unambiguous electron densities around 8-oxo-dGMP (supplemental Fig. S1*B* and Fig. 3*E*). The average *B* factor of 8-oxo-dGMP is 12.4 $Å^2$ and that of the residues involved in the recognition of 8-oxo-dGMP, Arg-23, His-28, Phe-35, Asp-77, Arg-78, and Asn-119 is 13.6 $Å^2$. These low *B* factors and unambiguous electron densities represent the small thermal motion and/or the ordered positioning of 8-oxo-dGMP and the residues of the active site in the crystal lattice. This phenomenon explains isothermal titration calorimetry experiments (45), indicating that the tight binding of 8-oxo-dGMP to MutT ($\Delta G = -9.8$ kcal/mol) is driven by a highly favorable enthalpy ($\Delta H = -39.0$ kcal/mol) with an unfavorable entropy ($-T\Delta S = 29.2$ kcal/mol). The unfavorable entropy would be a result of the conformational rigidity generated from the connection of loops L-A and L-D with large ligand-induced conformational changes. On the other hand, the more favorable enthalpy would be produced by the large number of hydrogen bonds and van der Waals interactions formed between 8-oxo-dGMP and MutT; this is sufficient to compensate for the unfavorable entropy and to bind tightly.

Furthermore, the hydrogen bond-mediated recognition mode found in MutT-8oxo-dGMP is comparable with the results of mutational studies in which it was found that the R78A, N119D, and N119A mutants show 7-, 37-, and 1650-fold decreases in affinity for 8-oxo-dGMP in comparison with the wild type and that they lose binding free energies ($\Delta\Delta G$) of 1.1, 2.1, and 4.3 kcal/mol, respectively, as measured by the increases in K_I (46). According to previous reports, the contribution of the hydrogen bond to protein stability can be estimated as ~2 and 1.2 kcal/mol for hydrogen bonds between protein residues

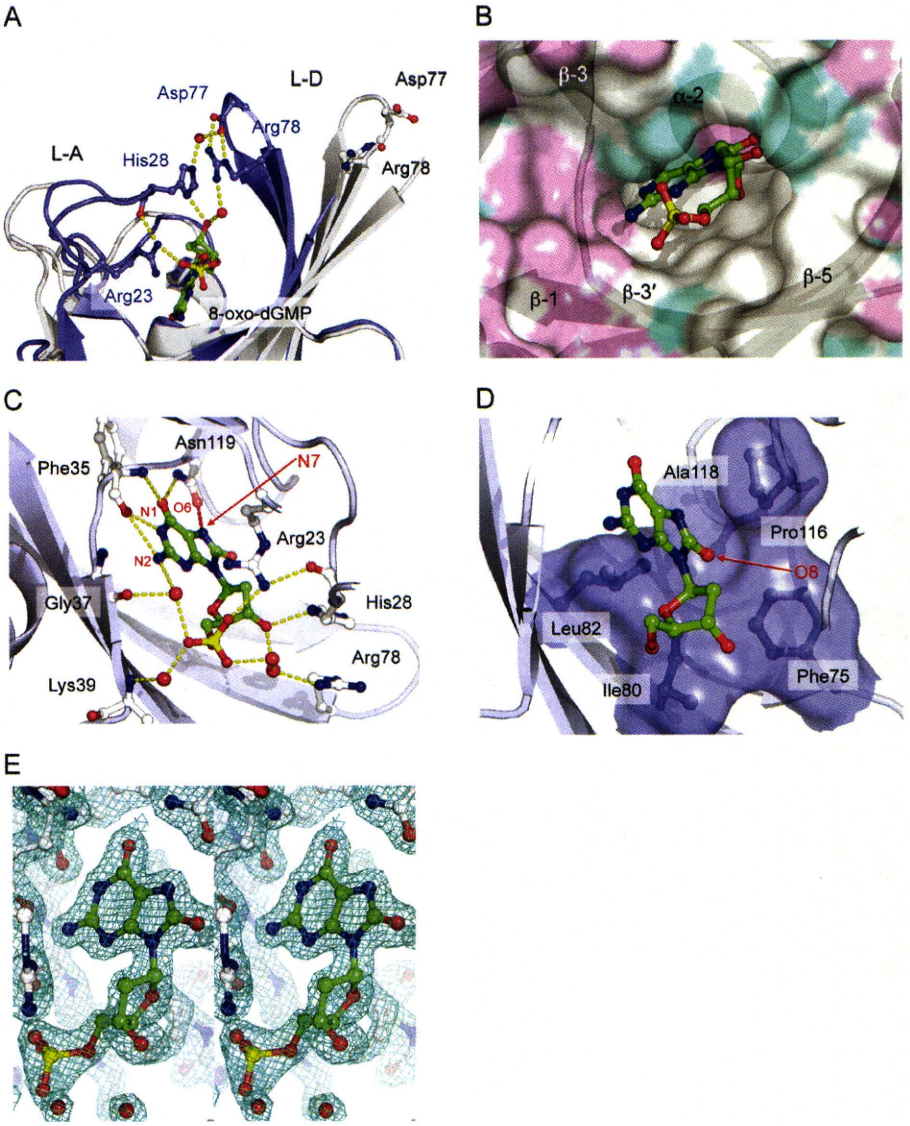

FIGURE 3. **Recognition of 8-oxo-dGMP by MutT.** *A*, hydrogen bonding interactions between 8-oxo-dGMP and loop regions (apo in *gray* and MutT-8-oxo-dGMP in *slate*). Amino acid residues involved in the hydrogen bonding interactions are shown in *ball and stick representation*. Water molecules are in *red*. Hydrogen bonds are shown as *yellow dashed lines*. *B*, the hydrophobic cave composed of β-1, β-3, β-3′, β-5, and α-2 is represented as a *translucent surface* (carbon in *white*, nitrogen in *cyan*, and oxygen in *pink*). *C*, interactions for the *syn* conformation of 8-oxo-dGMP. The hydrogen bond between Oδ of Asn-119 and N7-H of 8-oxoG is shown as a *red dashed line*. *D*, van der Waals interactions around the O8 atom. Amino acid residues recognizing O8 are shown in *ball, stick*, and *translucent surface*. *E*, a $2F_o - F_c$ electron density map around 8-oxo-dGMP contoured at 1.5 σ (*stereo view*).

and for those between a water molecule and a protein residue, respectively (47, 48). Judging from the MutT-8oxo-dGMP structure, the N119D and N119A mutants lose one hydrogen bond between the O6 of 8-oxo-dGMP and the Nδ-H of Asn-119 and two hydrogen bonds involving the O6 and N7-H of 8-oxo-dGMP and the amide group of Asn-119, respectively (Fig. 3*C*). The R78A mutant loses the hydrogen bond to a water molecule (Fig. 3*C*); that is, $\Delta\Delta G$ losses of 1.2, 2, and 4 kcal/mol are estimated for the R78A, N119D, and N119A mutants, respectively; this agrees perfectly with the experimental data (46).

The feature of the substrate-binding site in MutT-8-oxo-dGMP is also consistent with reports that MutT hydrolyzes both deoxyribose and ribose derivatives of 8-oxoG nucleotides with similar efficiency (2, 7). This is because, despite a number of hydrogen-bonding interactions between 8-oxo-dGMP and MutT, there is space for a hydroxyl group instead of the hydrogen atom at the 2′ position of the sugar ring (Fig. 3*B*). This recognition mechanism of 8-oxo-dGMP by MutT is different from any models predicted by NMR studies (PDB IDs: 1PPX, 1PUN, 1PUQ, 1PUS, and 1MUT) (supplemental Fig. S3).

Discrimination of 8-oxoG Nucleotides from G Nucleotides—The K_m values of *E. coli* MutT for 8-oxo-dGTP and 8-oxo-GTP are ~3,800- to 14,000-fold lower than the values for the corresponding G nucleotides (7). These data agree with the observation that the K_d value (52 nM) between 8-oxo-dGMP and MutT is 34,000-fold lower than that (1.76 mM) between dGMP and MutT (45). Thus, the most important question that this study addresses is the mechanism by which MutT obtains high substrate specificity for 8-oxoG nucleotides as compared with G nucleotides.

According to the recognition scheme of 8-oxo-dGMP by MutT, the major difference in the recognition of 8-oxoG *versus* G is whether the single hydrogen bond between Oδ of Asn-119 and N7-H of 8-oxoG occurs or not. This situation is similar to those of OGG1, MutM, and MutY (13, 15, 16). If the side-chain conformation of Asn-119 in the MutT complex with G nucleotides was the same as that in the MutT-8-oxo-dGMP structure, the two lone pairs at N7 of G and Oδ of Asn-119 would be repulsive (supplemental Fig. S4). To avoid this repulsion, a rotation about the side-chain torsion angles in Asn-119 should be required. Thus, the difference in the number of hydrogen bonds formed between MutT-G and MutT-8-oxoG complexes is only one. The contribution of one hydrogen bond to $\Delta\Delta G$ is estimated to be 2 kcal/mol (47, 48).

The *syn* glycosidic conformation of 8-oxo-dGMP must also be one of the elements contributing to the substrate specificity of MutT, because 8-oxoG nucleotides favor a *syn* conformation by the steric hindrance between O8 and the sugar moiety; this is in contrast with G nucleotides that adopt both *syn* and *anti* conformations (49, 50). Because of the lack of quantitative data